SIAM J. Applied Dynamical Systems
Vol. 9, No. 1, pp. 154–187


# Optimal Intrinsic Dynamics for Bursting in a Three-Cell Network*

Justin R. Dunmyre† and Jonathan E. Rubin‡

**Abstract.** Previous numerical and analytical work has shown that synaptic coupling can allow a network of model neurons to synchronize despite heterogeneity in intrinsic parameter values. In particular, synchronous bursting oscillations can arise in a network with excitatory synaptic coupling, even in the absence of intrinsically bursting neurons. In this work, we explore how the intrinsic dynamics of neurons within a reduced three-cell network influence its ability to exhibit synchronous bursting and the frequency range over which such activity can occur. We establish necessary and sufficient conditions for the existence of synchronous bursting solutions and perform related numerical experiments in three-cell networks that include a quiescent cell, a tonically active cell, and a third added cell. Our results show that, in most cases, the addition of a quiescent cell is optimal for synchronous network bursting, in a variety of ways, and that intrinsically bursting cells can be detrimental to synchronous bursting, and we explain the mechanisms underlying these effects. These findings may help explain how robust synchronous oscillations arise in neuronal central pattern generators, such as the mammalian inspiratory network, despite the presence of significant cellular heterogeneity. They also support the idea that intrinsic burst capabilities of individual cells need not be central to these networks' rhythms.

**Key words.** heterogeneous neuronal network, fast-slow decomposition, synaptic coupling, relaxation oscillations, respiratory network

**AMS subject classifications.** 34C15, 34C26, 37G15, 37N25, 70K70, 92C20

**DOI.** 10.1137/090765808

## 1. Introduction.

The pre-Bötzinger complex (preBötC) of the mammalian brainstem contains a collection of coupled neurons exhibiting robust, network-wide bursts of action potential firing under a considerable range of conditions [30]. These bursts may be responsible for controlling inspiratory respiration as well as gasping [19, 20, 29]. The preBötC is located within a ring of other networks, many of which provide inhibition to the preBötC. During phenomena like hypoxia, this inhibition may be released as the activation in these networks fades out, and so it falls on the preBötC to drive the respiratory rhythm [29, 25]. Thus, a significant component of understanding the respiratory cycle involves understanding the intrinsic dynamics of the preBötC. Experimental observations suggest that most cells in the preBötC, when considered in isolation, either are tonically active (firing spikes repeatedly) or are quiescent (spiking rarely if at all); however, there is also a significant population of cells that engage in intrinsic bursting behavior when they are decoupled from the rest of the network [8]. This

*Received by the editors July 21, 2009; accepted for publication (in revised form) by J. Sneyd November 4, 2009; published electronically February 19, 2010. This work was partially supported by NSF awards DMS-0716936 and EMSW21-RTG 0739261.
http://www.siam.org/journals/siads/9-1/76580.html
†Department of Mathematics and Complex Biological Systems Group, University of Pittsburgh, Pittsburgh, PA 15260 (mathemagician@gmail.com).
‡Department of Mathematics and Complex Biological Systems Group and Center for the Neural Basis of Cognition, University of Pittsburgh, Pittsburgh, PA 15260 (rubin@math.pitt.edu).

work attempts to answer the question of what the role of these neurons that burst in isolation might be in the control of preBötC dynamics.

In [3, 4], Butera, Rinzel, and Smith developed an ODE model of a class of neurons in the preBötC characterized by the presence of a persistent sodium current. Working with the model from [3, 4], Rubin provided conditions for the emergence of synchronous bursting in a pair of burst-capable cells, one tuned to be intrinsically quiescent and the other to be intrinsically tonic, coupled with synaptic excitation [27], thereby proving that burst-capable neurons need not be tuned to be intrinsically bursting in the absence of inputs in order for them to generate network bursting when coupled (see also [23]). Purvis et al. used simulations of a network including a mixture of intrinsically burst-capable and burst-incapable cells to show that the presence of significant numbers of burst-capable cells enhances the parameter range over which synchronous bursts occur and the frequency range that bursts achieve under modulation of a control parameter [21]. Together, these findings highlight the importance of burst-capable cells for synchronous bursting within the preBötC but also lead us to ask, given that cells that are tuned to burst in isolation are not necessary for network-wide synchronous bursting, how do they contribute to such activity patterns?

Given the heterogeneity of dynamics observed in isolated preBötC cells (see also [22]) and the evidence for the involvement of burst-capable cells in network activity, we explore the role of intrinsically bursting cells in the preBötC by considering heterogenous networks, each containing three burst-capable cells. Such networks are large enough to include representatives of all three types of intrinsic dynamics (quiescence, bursting, and tonic spiking), and hence for the role of intrinsically bursting cells in a heterogeneous network to become apparent, but are also small enough to allow for the analysis of the dynamic effects of the presence of intrinsic bursters.

Including this introduction and the appendices, this work is partitioned into eight sections. Section 2 introduces the model we will use for our analysis and provides a heuristic introduction to the theory of relaxation oscillators, including the effects of synaptic coupling. Section 3 provides a set of necessary conditions for periodic, synchronous bursting oscillations to occur within our three-cell network, as well as a separate set of sufficient conditions for such a solution to exist in the network. Although these conditions are presented for a three-cell network, the interested reader may refer to Appendix B, which provides a guideline for extending these conditions to an arbitrarily sized network. Section 4 provides results and analysis of two numerical experiments. The first experiment explores which cells promote synchronous oscillations if added to a network already containing an intrinsically quiescent and an intrinsically tonic cell. The second simulation addresses the issue of frequency control in the three-cell network. Finally, we summarize our work and suggest directions for future research in the discussion contained in section 5.

## 2. Introductory theory.

**2.1. Models.** Throughout this work, we will focus on a reduced version of the model developed by Butera and colleagues [3, 4]. The original model for an individual cell in isolation is

$$v' = (-I_{NaP}(h,v) - I_{Na}(n,v) - I_K(n,v) - I_L(v) - I_{tonic-e}(v) + I_{app})/C_m, \tag{1}$$

$$n' = (n_\infty(v) - n)/\tau_n(v), \tag{2}$$

$$h' = \varepsilon(h_\infty(v) - h)/\tau_h(v), \tag{3}$$

$$s' = \alpha_s(1 - s)s_\infty(v) - s/\tau_s, \tag{4}$$

with $I_{NaP}(h, v) = g_{NaP}m_{p,\infty}(v)h(v-E_{Na})$, $I_{Na}(n, v) = g_{Na}m^3_\infty(v)(1-n)(v-E_{Na})$, $I_K(n, v) = g_K n^4(v - E_K)$, $I_L(v) = g_L(v - E_L)$, and $I_{tonic-e} = g_{ton}(v - E_{syn-e})$. Equation (4) relates to the strength of synaptic signals generated by the cell. The variable $s$ does not feed back to (1)–(3) in the isolated cell case but will play an important role in coupled networks later in the paper. Values for the parameters and the definitions of the other functions appearing in this model can be found in Appendix A. Typically, the small parameter $\varepsilon$ is absorbed into the function $\tau_h(v)$; however, for clarity of analysis, we have factored it out.

Neurons modeled by these equations are classified as quiescent, bursting, or tonic, depending on their activity patterns. After a transient that depends on the initial conditions of the system, a quiescent neuron will not spike, and a tonic neuron will repeatedly fire spikes at a regular frequency. A bursting neuron will switch between active and silent phases. During the active phase a bursting neuron emits spikes, while during the silent phase it does not. Thus, a quiescent neuron can be thought of as being stuck in the silent phase, while a tonic neuron is stuck in the active phase. Depending on the relative magnitudes of its ionic conductances, each quiescent or tonic cell may be burst-capable, meaning that it can burst for some level of $g_{ton}$, or not; for example, a large $g_L$ relative to $g_{NaP}$, or vice versa, can eliminate burst-capability.

In the given model, when the neuron is in the active phase, the currents $I_K$ and $I_{Na}$ are what cause the rapid fluctuations in the $v$ variable that we interpret as spikes. In the silent phase, these currents do not contribute much to the $v$ dynamics. Removing these terms from the $v$ equation also allows us to remove (2) to obtain a reduced model that is more amenable to analysis. This reduced model has been used previously for the analysis of synchronous oscillations in a heterogeneous network combining intrinsically bursting and intrinsically quiescent cells, as well as for a coupled intrinsically quiescent and intrinsically tonic cell pair [26, 27]. The model takes the form

$$v' = (-I_{NaP}(h, v) - I_L(v) - I_{tonic-e}(v) + I_{app})/C_m, \tag{5}$$

$$h' = \varepsilon(h_\infty(v) - h)/\tau_h(v), \tag{6}$$

$$s' = \alpha_s(1 - s)s_\infty(v) - s/\tau_s, \tag{7}$$

where $I_{NaP}(h, v)$ and $I_L(v)$ are as given above.

The $s$ variable in (7) is slaved to $v$, and it does not appear in (5) and (6), so it is useful to do analysis on the $vh$ phase plane. A nice feature of this reduced model is that if we make biologically reasonable assumptions on the parameters, then (5) and (7) operate on a fast time scale, while (6) evolves on a slow time scale, due to the small size of $\varepsilon$. Further, within a broad, biologically relevant parameter range, the $v$-nullcline (the algebraic equation $v' = 0$) can be written as a twice differentiable function $F(v)$ with a cubic shape, while the $h$-nullcline is a sigmoidal curve that is monotone decreasing as a function of $v$. We follow the work of Rubin in [27] to perform analysis on this model. Insights based on the shapes and positions of the nullclines often suffice to analyze the model. When $F(v)$ is cubic, we call its branches the

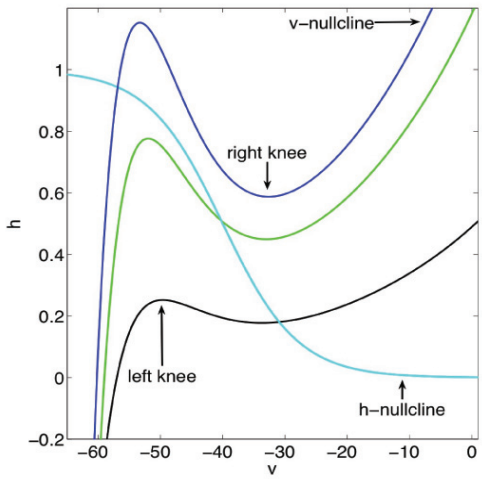


**Figure 1.** *Example nullclines for three different instances of the reduced model. For $\varepsilon$ sufficiently small, the dark blue nullcline corresponds to a quiescent cell, the green nullcline represents a bursting cell, and the black nullcline represents a tonic cell. All three cells in this case share the same h-nullcline, which is light blue. All parameters are as in Table 3, except that for the quiescent cell we have $g_{NaP} = 2, g_L = 2.5$, for the bursting cell we have $g_{NaP} = 2, g_L = 2$, and for the tonic cell we have $g_{NaP} = 3.5, g_L = 1.5$.*

left, middle, and right branches, respectively. The left branch satisfies $F'(v) > 0, F''(v) < 0$; the middle branch has $F'(v) < 0$; and the right branch has $F'(v) > 0, F''(v) > 0$. Where the left branch meets the middle branch there is a local maximum of the nullcline, which we will call the left knee. Similarly, where the middle branch meets the right branch there is a local minimum of the nullcline, which we will call the right knee. See Figure 1 for an example chosen to illustrate these definitions. If we make a further assumption that the nullclines intersect exactly once, then it is a straightforward calculation to determine the stability of the resulting critical point.

**2.2. Review of the dynamics of a relaxation oscillator.** In this subsection we simply provide a brief, heuristic discussion of relaxation oscillator dynamics relevant for our analysis of system (5)–(6). Analysis of the dynamics of relaxation oscillators in arbitrary dimensions can be done using the tools of geometric singular perturbation theory [9, 17, 14].

For $0 < \varepsilon \ll 1$ and $v \in \mathbb{R},\ h \in \mathbb{R}$ consider a system of the form

$$v' = f(v, h), \tag{8}$$

$$h' = \varepsilon g(v, h). \tag{9}$$

Suppose further that the $v$-nullcline can be written as a cubic-shaped function $h = F(v)$ with $\lim_{v\to\infty} F(v) = \infty$. Allow the $h$-nullcline to be a monotonically decreasing function of $v$. We will again use the terminology from section 2.1 to describe the knees and branches of the $v$-nullcline; see Figure 1. Figure 1 contains three different $v$-nullclines, one where the intersection with the $h$-nullcline is on the left branch, another where the intersection is on the middle branch, and a last one where the intersection falls on the right branch. If the

$h$-nullcline intersects the $v$-nullcline near one of the knees, we risk the existence of canards, which are outside of the scope of this work. Let $(v_p, h_p)$ be the intersection point of the $v$ and $h$-nullclines, and let $(v_{LK}, h_{LK}), (v_{RK}, h_{RK})$ denote the left and right knees, respectively. For a given $\varepsilon > 0$ there is a $\delta = \delta(\varepsilon) > 0$ such that if $\min\{|v_p - v_{LK}|, |v_p - v_{RK}|\} > \delta$, then canards will not exist. For the remainder of the work, we assume that this inequality holds.

It is useful at this point to define a way to measure the distance of a point from the $v$-nullcline. For any fixed $h$ there are between one and three values of $v$ such that $F(v) = h$. We will concern ourselves only with those $v$ that correspond to the left and right branches of the $v$-nullcline. Allow $v_{LB}(h)$ to be the $v$ such that $F(v_{LB}) = h$ and $(v_{LB}, h)$ is on the left branch of the $v$-nullcline, and if there is no such $v$, then set $v_{LB}(h) = \infty$. Similarly, allow $v_{RB}(h)$ to be the value of $v$ such that $F(v_{RB}) = h$ and $(v_{RB}, h)$ is on the right branch of the $v$-nullcline, and set $v_{RB}(h) = \infty$ if no such $v$ exists. Let $\Gamma_v(t)$ be the $v$-coordinate at time $t$ of a trajectory $\Gamma(t)$ of the ODE. Similarly, allow $\Gamma_h(t)$ to be the $h$-coordinate at time $t$ for the trajectory $\Gamma(t)$. Now we can define the distance from $\Gamma(t)$ to the $v$-nullcline as $D(\Gamma(t)) = \min\{|\Gamma_v(t) - v_{LB}(\Gamma_h(t))|, |\Gamma_v(t) - v_{RB}(\Gamma_h(t))|\}$.

The intersection of the $v$ and $h$-nullclines is a critical point of system (8)–(9). Suppose now that $v' < 0$ below the $v$-nullcline and $v' > 0$ above it. Similarly, assume that $h' > 0$ below the $h$-nullcline and $h' < 0$ above it. These assumptions, together with the critical point being bounded away from the knees, imply that critical points on the middle branch of the $v$-nullcline are unstable, while critical points on the left and right branches of the $v$-nullcline are stable. If for some time $t$, $D(\Gamma(t))$ is large relative to $\varepsilon$, then $|v'| \gg 0$ and comparatively $h' \approx 0$. So we consider that the dynamics hold $h$ fixed, and $\Gamma(t)$ quickly approaches a neighborhood of the $v$-nullcline for this fixed $h$. Once $D(\Gamma(t))$ is small enough, then $|v'| \approx 0$, and the $h$ dynamics become relevant.

First, consider the case that the critical point lies on the middle branch of the $v$-nullcline. Suppose we start with $\Gamma(0)$ on the left branch of the $v$-nullcline. Since the critical point is on the middle branch of the $v$-nullcline, $\Gamma_h(0)$ is below the $h$-nullcline, and so $\Gamma_h'(0) > 0$. The $\varepsilon$ in (9) implies that the $h$ dynamics are slow, so we say that the trajectory oozes up toward the $h$-nullcline, remaining close to the $v$-nullcline. Eventually $\Gamma_h(t) > h_{LK}$. In this situation, we find that $D(\Gamma(t))$ is large, because for $\Gamma_h(t)$ there is only one corresponding point on the $v$-nullcline, and it is on the right branch. So suddenly $\Gamma_v'(t) \gg 0$, and the trajectory quickly jumps over to the right branch of the $v$-nullcline, with $\Gamma_h(t)$ barely changing. Now $\Gamma_h(t)$ is above the $h$-nullcline, so $\Gamma(t)$ begins to ooze down toward the right knee. Since the $h$-nullcline is below the right knee, $\Gamma$(t) will eventually drift below the right knee, and as before, it is suddenly the case that $D(\Gamma(t)) \gg 0$. So $\Gamma$(t) will quickly fall down to the left branch of the $v$-nullcline, completing one cycle. This alternation of prolonged phases of slow change interrupted by fast transitions between phases is the hallmark of relaxation oscillations. In the two-dimensional case, the Poincaré–Bendixon theorem implies the existence of periodic relaxation oscillations in this situation.

Suppose instead that the critical point is on the left branch of the $v$-nullcline. If $\Gamma(t)$ is on the right branch of the $v$-nullcline, it will ooze down until it drifts below the right knee, at which point it falls down to the left branch of the $v$-nullcline, as before. However, since the critical point on the left branch of the $v$-nullcline is asymptotically stable, the trajectory will not be able to get above the left knee. So instead of jumping back to the right branch of the

$v$-nullcline, the trajectory simply approaches the critical point. Similarly, if the critical point is on the right branch of the $v$-nullcline, the trajectory will eventually converge to the critical point.

The $v$-nullcline for (1) or (5) may or may not be cubic, depending on parameters such as $g_L$ and $g_{NaP}$. In either case, in the full model (1)–(4), spiking activity evolves due to the $I_K$ and $I_{Na}$ currents, and spiking occurs for $v$ only above some threshold. This spiking behavior is encoded in the reduced model by the variable $s$, representing synaptic output. We see that (7) involves $s_\infty(v)$, which is a steep sigmoidal function (Appendix A) since $\sigma_s$ is small. $s_\infty(v)$ takes the value $\frac{1}{2}$ at $v = \theta_s$, which we call the synaptic threshold. For values of $v$ arising during spiking, corresponding to the right branch of the $v$-nullcline when it is cubic, $s_\infty(v) \approx 1$, and the cell is producing synaptic output as would be generated with spiking in the full model. On the other hand, for values of $v$ arising when the cell is quiescent, corresponding to the left branch of the $v$-nullcline when it is cubic, $s_\infty(v) \approx 0$, representing an absence of spiking. Should the $v$-nullcline be cubic with a critical point on its middle branch, the cell will oscillate between phases of low $s$ and phases of $s \approx s_{max}$, corresponding to intrinsic bursting. We will use the location of the critical point to classify our modeled cells as intrinsically bursting (cubic $v$-nullcline with critical point on its middle branch), quiescent (cubic $v$-nullcline with critical point on its left branch or monotone $v$-nullcline with critical point below $\theta_s$), or tonic (cubic $v$-nullcline with critical point on its right branch or monotone $v$-nullcline with critical point above $\theta_s$).

**2.3. Heterogeneity in $g_{NaP}$ and $g_L$.** The preBötC is a heterogeneous network of cells that are quiescent, tonically active, or bursting in isolation [8]. Following [21], in order to reflect this heterogeneity in our work, we consider heterogeneity in two parameters: the conductance $g_{NaP}$ of the persistent sodium current $I_{NaP}$ and the conductance $g_L$ of the leak current $I_L$. Increasing $g_L$ has the effect of raising the entire $v$-nullcline, in particular, the left knee. This moves the intersection of the $v$- and $h$-nullclines to lower $v$ values. Numerically, we observe that increasing $g_{NaP}$ has the effect of moving the intersection of the $v$- and $h$-nullclines to higher $v$ values. Below, in Figure 2, we show the partitioning of $g_{NaP}g_L$ space into regions where the resultant cell is quiescent (blue), bursting (green), or tonically active (black). For each $g_{NaP}g_L$ pair, we find the branch on which the $h$-nullcline intersects the $v$-nullcline if the nullcline is cubic on $0 \le h \le 1$. If the intersection is on the left, middle, or right branch, the cell is declared quiescent, bursting, or tonic, and is colored blue, green, or black, respectively. The coloring in Figure 2 does not take into account those small neighborhoods around the knee where the intersection of the nullclines may result in a canard explosion, or where the Andronov–Hopf bifurcation does not occur precisely at the knee, as these cases only occur on very small parameter ranges, due to the disparity in time scales of $v$ and $h$, and thus are not significant for our results. If the $v$-nullcline is not cubic (e.g., large $g_{NaP}$ relative to $g_L$) or if it is only single branched for $0 \le h \le 1$ (e.g., large $g_L$ relative to $g_{NaP}$), then we classify the cell as quiescent or tonic depending on the position of the critical point relative to the synaptic threshold, $\theta_s$. Further detail on the effects of varying $g_{NaP}$ and $g_L$ can be found in section 4.3.

**2.4. Effects of synaptic coupling.** In a network of coupled cells, each individual cell in the network will have its own $v$, $h$, and $s$ variables. The rest of this work concerns a network

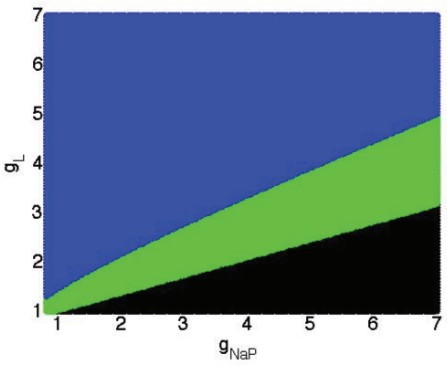


**Figure 2.** *Partitioning of $g_{NaP}g_L$ space into regions where the cells are quiescent (blue), bursting (greeen), or tonic (black).*

of three cells, so for $i = 1, 2, 3$, we adopt the vector notation $cell_i = [v_i, h_i, s_i]$, where

$$(10)\quad v_i' = \left( -I_{NaP,i}(h_i, v_i) - I_{L,i}(v_i) - I_{tonic-e}(v_i) + I_{app} - \sum_{j \neq i} g_{ij} s_j (v_i - E_{syn-e}) \right) / C_m,$$

$$(11)\quad h_i' = \varepsilon (h_\infty(v_i) - h_i)/\tau_h(v_i),$$

$$(12)\quad s_i' = \alpha_s (1 - s_i) s_\infty(v_i) - s_i/\tau_s,$$

with $I_{NaP,i}(v_i, h_i) = g_{NaP,i} m_{p,\infty}(v_i) h_i (v_i - E_{Na})$, $I_{L,i}(v_i) = g_{L,i}(v_i - E_L)$, and $I_{tonic-e}(v_i) = g_{ton}(v_i - E_{syn-e})$. Note that (10) excludes self-coupling, yet self-coupling could easily be included in the analysis if desired (see Appendix B). We henceforth assume that the $v$-nullcline for each neuron is cubic, with associated active and silent phases corresponding to its right and left branches, respectively, since this assumption is violated only on the edges of the parameter range illustrated in Figure 2, away from where the important dynamic effects occur.

In section 3.2 we will prove that when $s_j$ increases, the knees of the coupled cells have lower $h_i$ coordinates; see Figure 3. Here, we will use this result, without proof, to briefly illustrate the mechanism by which a network of these modeled neurons may produce synchronous bursts. We continue to assume that $\varepsilon$ is small so that the $h$ dynamics are slow relative to the $v$ and $s$ dynamics; see section 2.2. Thus, in a network architecture where $cell_1 = [v_1, h_1, s_1]$ is coupled to $cell_2 = [v_2, h_2, s_2]$ and both cells are initially in the silent phase, if the trajectory for $cell_1$ transitions to the active phase, then there is an instantaneous change in the $v_2$-nullcline. It may happen that the left knee for $cell_2$ has dropped below the current value of $h_2$, in which case $cell_2$ immediately transitions to the active phase. A similar effect may happen when one cell transitions to the silent phase. Such fast threshold modulation [31] can yield rapid convergence to synchronous oscillations by allowing the trailing cell to catch up to the cell ahead of it, although order switching may complicate the dynamics. A great amount of detail on this mechanism is provided in [27, 2, 31, 26].

**2.5. Illustration of three coupled cells.** In this section, we illustrate how the dynamics in which we are interested, synchronous bursting, can arise in an all-to-all coupled network of

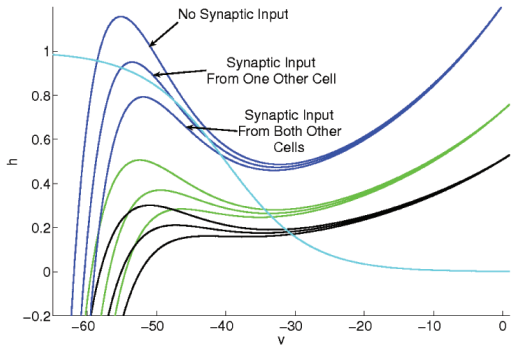


**Figure 3.** *Various levels of synaptic input to sample instances of the reduced model. The blue, green, and black nullclines represent, respectively, a quiescent, a bursting, and a tonic cell under various levels of synaptic input. The key feature is that synaptic input from another cell lowers both the left and the right knee of the receiving cell. In this way, a quiescent cell can become bursting, and a bursting cell can become tonic.*

three cells, modeled by (10)–(12), with heterogeneity introduced through $g_{NaP}$ and $g_L$, such that one cell is intrinsically quiescent, one is intrinsically bursting, and one is intrinsically tonic. We define a solution as a synchronous bursting oscillation if all three cells transition repeatedly, via fast excursions controlled by their $v$ dynamics, between the silent and active phases, and, after one cell undergoes a transition from one phase to another, all the other cells join it in its new phase before any cell undergoes a transition out of that phase. We will study this system by projecting the solution onto three separate phase planes, $(v_1, h_1)$, $(v_2, h_2)$, and $(v_3, h_3)$, while keeping in mind that the position of $v_j$ in the $(v_j, h_j)$ phase plane directly affects $s_j$ and so changes the shapes of the $v$-nullclines in the other two phase planes. Suppose that in the absence of coupling, $cell_1$ is quiescent, $cell_2$ is bursting, and $cell_3$ is tonic. We will use the shorthand $Q$, $B$, and $T$, for $cell_1$, $cell_2$, and $cell_3$, respectively. We start with all three cells in the silent phase, and view the evolution of the trajectory as a series of snapshots, laid out in Figures 4–15. Though the $v_j$-nullclines actually change continuously as a function of $v_i$ for $i \neq j$, we assume that the change is fast enough to be considered instantaneous relative to the slow $h$ dynamics.

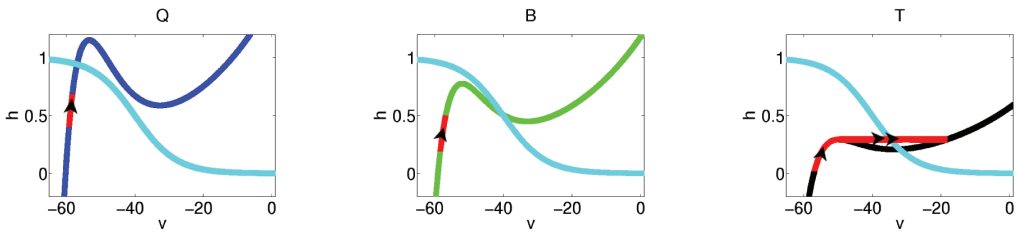


**Figure 4.** *Starting with all cells silent, $T$ is the first to reach its left knee and enter the active phase. In this figure and for Figures 5–15, the dark blue, green, and black curves represent the $v$-nullclines for the $Q$, $B$, and $T$ cells, respectively. The light blue curve is the $h$-nullcline. Red represents the trajectory of the system. One black arrow indicates slow evolution, while two black arrows indicates a fast evolution.*

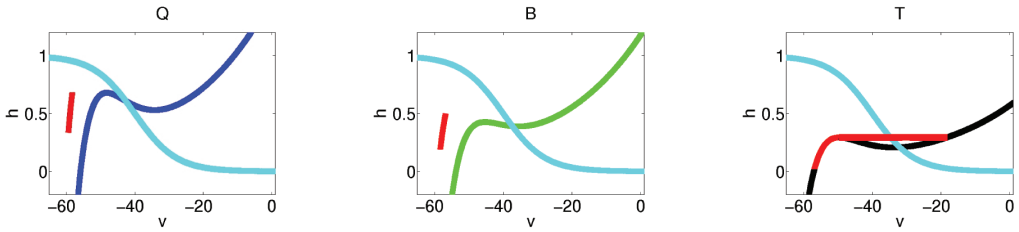


**Figure 5.** *Now that $T$ is in the active phase, it sends synaptic input to the other two cells, and their $v$-nullclines change abruptly.*

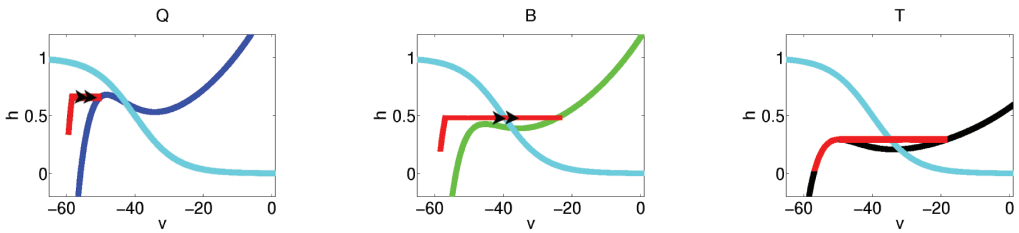


**Figure 6.** *Due to the synaptic input from $T$, $B$ is suddenly above its left knee, so it immediately enters the active phase. Meanwhile, $Q$ quickly approaches its $v$-nullcline.*

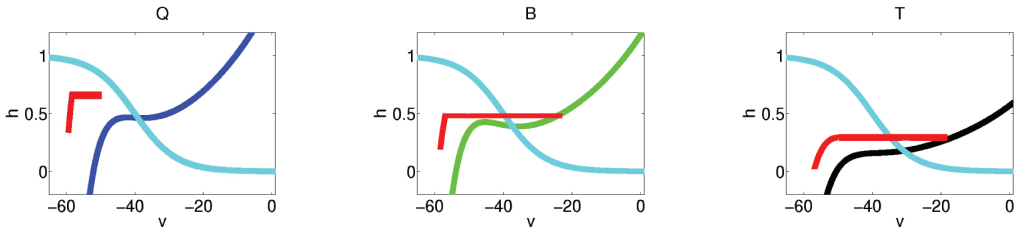


**Figure 7.** *Now that $B$ is in the active phase, it sends synaptic input to both $Q$ and $T$, and their $v$-nullclines are updated accordingly.*

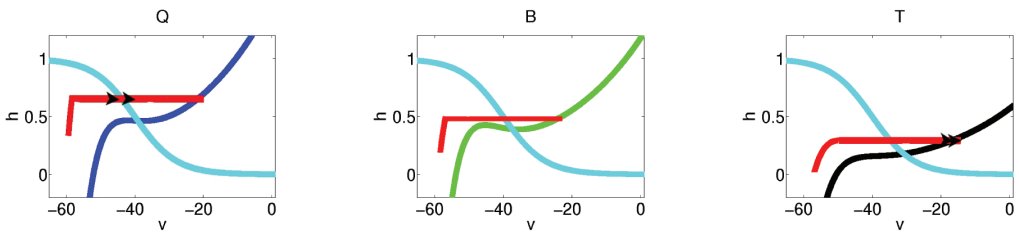


**Figure 8.** *$Q$ is now above its left knee, and so it enters the active phase.*

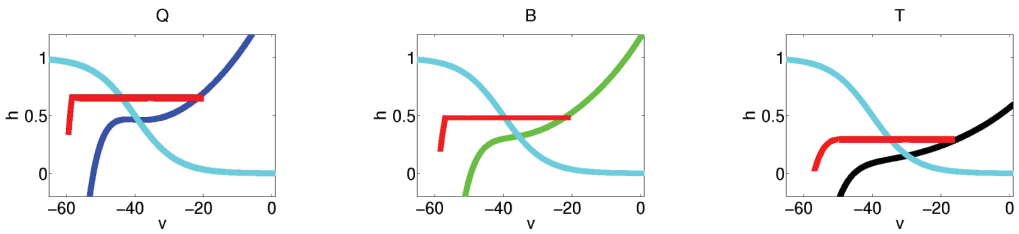


**Figure 9.** *Now that Q is in the active phase, it sends synaptic signals to B and T, so their v-nullclines are updated.*

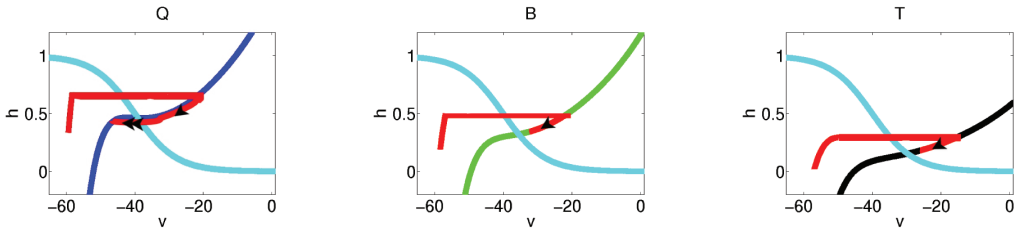


**Figure 10.** *The system evolves until one of the cells reaches its right knee. In this case, the Q cell must be the first to do so, because the other two cells become tonic under the current input levels.*

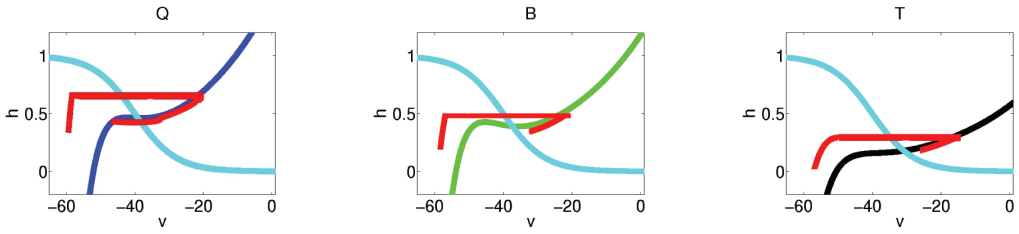


**Figure 11.** *Q has returned to the silent phase, so the v-nullclines are updated for cells B and T.*

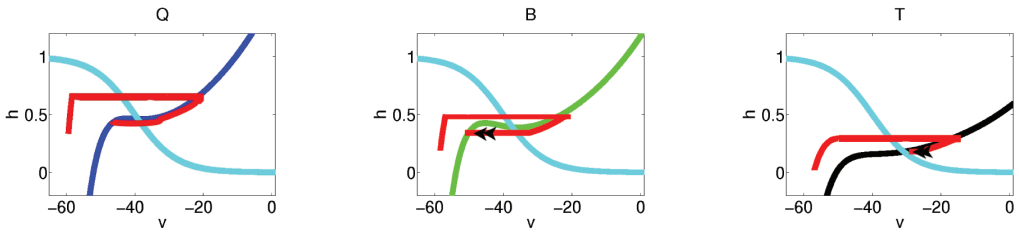


**Figure 12.** *With the synaptic input from Q removed, B is below its right knee and enters the silent phase.*

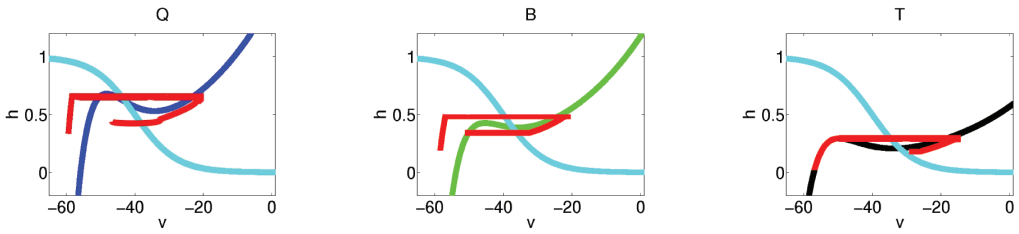


**Figure 13.** *Now that B is in the silent phase, synaptic inputs to Q and T are removed, and their v-nullclines are updated.*

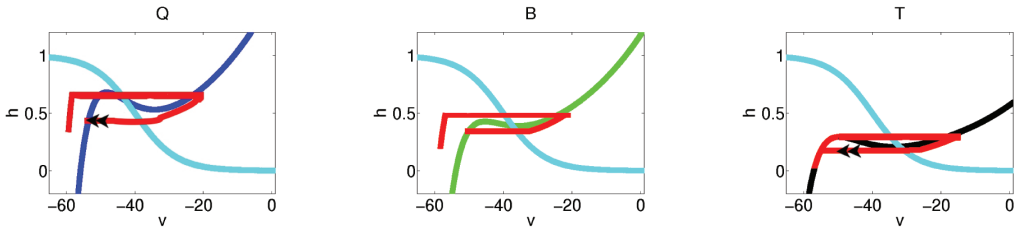


**Figure 14.** *Finally T is below its right knee, so it falls down to the silent phase.*

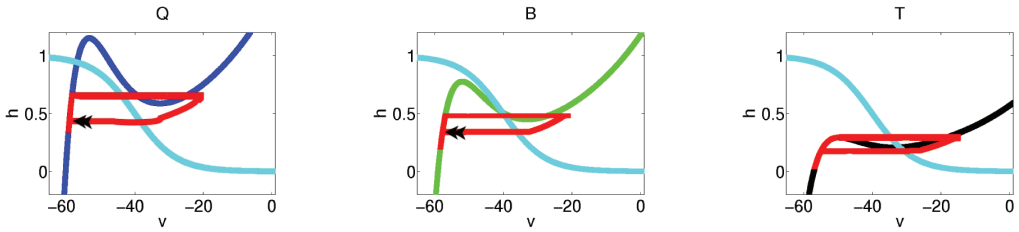


**Figure 15.** *All cells have returned to the silent phase, so all synaptic inputs are removed. This completes one cycle of the oscillation.*

**2.6. Remarks on synaptic adaptation.** The cartoon presented in Figures 4–15 omits one feature of (12). Typically, $s_\infty(v)$ is a sigmoidal function. However, if the sigmoid is not steep, then there is a significant range of values of $v$ where the synaptic output of the cell is reduced from its maximal value but remains nonzero. This effect can represent synaptic adaptation, if the relevant range of $v$-values overlaps the right branch of the $v$-nullcline (i.e., the active phase). That is, $v$ effectively evolves on the slow time scale for a cell on the right branch, and a slow change in $v$ yields a slow change in $s$ and hence a gradual change in the $v$-nullclines of the other cells. This may have far-reaching ramifications; for instance, if the $v$-nullcline of a quiescent cell does not change fast enough, then the cell may not be able to transition to the active phase. Further consideration of the effects of synaptic adaptation can be found in [32, 7].

## 3. Synchronous oscillations in three-cell networks.

**3.1. Necessary conditions for synchronous bursting.** Our definition of synchronous does not require cells to transition between the active and silent phases at precisely the same time. Instead, we call a solution synchronous if the following conditions are always met after some transient time. When $cell_i$ transitions to the active phase, every other $cell_j$, for $j \neq i$, must have been in the active phase before $cell_i$ returns to the silent phase. Similarly, after the return to the silent phase, $cell_i$ does not transition to the active phase until all other cells have visited the silent phase. For an $n$-cell network, these conditions can be formulated in terms of the time it takes each cell to reach the left or right knee, as appropriate.

We will consider iterations on two sets of integers, one set containing the indices of cells in the active phase, the other set containing the indices of cells in the silent phase. An iteration involves moving an index between the two sets. We let $i \in S_m \subseteq \{1, 2, \ldots, n\}$ if $cell_i$ is in the silent phase at iteration $m$. Similarly, $i \in A_m \subseteq \{1, 2, \ldots, n\}$ if $cell_i$ is in the active phase at iteration $m$. Let $T_{LK}(i, m)$ be the time it takes $cell_i$ to reach the left knee from its current position, which depends heavily on the current state of the network, implicitly encoded in the iteration number $m$. Similarly define $T_{RK}(i, m)$ as the time it takes $cell_i$ to reach the right knee from its current position in iteration $m$. There are two network-wide stages to consider: the first is "cells are transitioning from the silent to the active phase," and the other is "cells are transitioning from the active to the silent phase." Assume that $S_0 = \{1, 2, \ldots, n\}$ and $A_0 = \emptyset$. Let $k$ be the index such that $k = \text{argmin}_{i\in\{1,2,\ldots,n\}} T_{LK}(i, 0)$. Then we write $S_1 = S_0 \backslash k$ and $A_1 = A_0 \cup k$. This completes one iteration on the sets. We then consider the system again after time $T_{LK}(k, 0)$.

With this notation, the necessary condition that no cell in the active phase may return to the silent phase until there are no cells in the silent phase during the $m$th iteration can be phrased as

$$\inf_{i\in S_m} \{T_{LK}(i, m)\} < \inf_{j\in A_m} \{T_{RK}(j, m)\}. \tag{13}$$

That is, for fixed $m$, as long as (13) holds, the first cell to jump up can be moved from $S_m$ to $A_{m+1}$ to complete the $m$th iteration. If (13) holds for $m = 0, 1, \ldots, n-1$, then all cells enter the active phase before any cell leaves it. Then, after the first cell returns to the silent phase, the condition is reversed for the "cells returning to the silent phase" network stage. We must have $\inf_{j\in A_m}\{T_{RK}(j, m)\} < \inf_{i\in S_m}\{T_{LK}(i, m)\}$ in this case, until all cells are back to the silent phase. In order for a network to maintain synchronous bursting, these conditions must be satisfied for all $m \in \mathbb{N}$.

*Remark.* For fast-slow networks of arbitrary size, classification of cells into finer bins, depending on slow variable values in the silent phase, can be used to develop a Markov chain representation of network dynamics [24]. For the study of synchronous bursting solutions as we have defined them, two bins suffice.

**3.2. Sufficient conditions for synchronous bursting.** In this section we provide sufficient conditions for the existence of synchronous bursting oscillations in a three-cell network of cells with all-to-all coupling modeled by (10)–(12). The results in this section generalize to networks with an arbitrary number of cells with all-to-all coupling. The technique used can

also be generalized to other architectures; see Appendix B for details. Also for convenience, we assume that one cell in this network is intrinsically quiescent and another cell is tonic in the absence of input. We will place some restrictions on the third cell, again for notational convenience. These restrictions will arise in the context of the proof. The proof that the provided conditions are sufficient for synchronous bursting works in the $\varepsilon = 0$ limit, though with sufficient effort it may be extended to $0 < \varepsilon \ll 1$; see [17]. We also assume without loss of generality that $g_{ton} = 0$, because the arguments below are based on the shapes of the nullclines and the times of flight, which are qualitatively independent of $g_{ton}$.

Suppose that $j \in \mathbb{Z}_3$. Let $j = 0$ correspond to the intrinsically quiescent cell, which we shall also call $Q$ for short. Let $j = 2$ correspond to the intrinsically tonic cell, also called $T$ below. Further, $j = 1$ will denote the other cell, which we will abbreviate by $A$ for "added." The architecture is such that cell $j$ receives synaptic input from cells $j-1$ and $j+1$.

In the $\varepsilon = 0$ limit, the dynamics for $v_j$ and $s_j$ are reduced to algebraic equations, and the $h_j$ dynamics become relevant. For a fixed $s_{j-1}$ and $s_{j+1}$ and a given $h_j$, there are up to three corresponding values of $v_j$, one for each branch of the $v_j$-nullcline. However, if we restrict our view to each branch individually, the monotonic nature of these branches permits us to write $v_j = v_j^X(h_j, s_{j-1}, s_{j+1})$ for $X \in \{L, M, R\}$. Further, since $s_j$ can be considered as a function of $v_j$, we can write $s_j = s_j^X(h_j, s_{j-1}, s_{j+1})$ for $X \in \{L, M, R\}$. Since there are three cells and each could be on either the left or right branch of the $v$-nullcline, there are many possible slow subsystems. Due to the algebraic dependencies detailed above, to describe the dynamics for $\overrightarrow{h} = [h_0, h_1, h_2]$, we use the notation $\dot{\overrightarrow{h}} = G_{XYZ}(h)$ if $v_0$, $v_1$, $v_2$ are on the $X$, $Y$, $Z$ branches of their respective $v$-nullclines, for $X, Y, Z \in \{L, M, R\}$.

For each cell $j$ we label the $h$ coordinate of the left knee, right knee, and fixed point by $LK(s_{j-1}, s_{j+1}; j), RK(s_{j-1}, s_{j+1}; j), FP(s_{j-1}, s_{j+1}; j)$, respectively. Below, we justify this functional notation by the implicit function theorem. We will carry through the analysis for (10)–(12), though it is clear that the techniques apply to any model with similar structure.

Lemma 3.1. *The $h$-coordinates of the left and right knees and the fixed point of cell$_j$, modeled by (10)–(12), are monotonically decreasing functions of the synaptic input variables $s_{j-1}$ and $s_{j+1}$.*

*Proof.* Note that $v_j$ obeys the equation

$$\begin{aligned} \dot{v_j} = \big( &- g_{NaP} m_{P,\infty}(v_j)(v_j - E_{Na}) h_j - g_L(v_j - E_L) \\ &- g_{j,j-1} s_{j-1}(v_j - E_{syn-e}) - g_{j,j+1} s_{j+1}(v_j - E_{syn-e}) \big)/C_m. \end{aligned} \tag{14}$$

We solve $\dot{v_j} = 0$ for $h_j$ to find $F(v_j, s_{j-1}, s_{j+1})$, the $v$-nullcline:

$$h_j = F(v_j, s_{j-1}, s_{j+1}) := \frac{-g_{j,j-1} s_{j-1}(v_j - E_{syn-e}) - g_{j,j+1} s_{j+1}(v_j - E_{syn-e}) - g_L(v_j - E_L)}{g_{NaP} m_{p,\infty}(v_j)(v_j - E_{Na})}. \tag{15}$$

For fixed synaptic input variables $s_{j-1}^*$, $s_{j+1}^*$, the $v$-coordinate of the right knee of cell $j$,

denoted by $v_j^{RK}$, satisfies

$$\left.\frac{\partial F}{\partial v_j}\right|_{(v_j^{RK},s_{j-1}^*,s_{j+1}^*)} =: F_{v_j}(v_j^{RK},s_{j-1}^*,s_{j+1}^*) = 0,$$
$$\left.\frac{\partial^2 F}{\partial v_j^2}\right|_{(v_j^{RK},s_{j-1}^*,s_{j+1}^*)} =: F_{v_jv_j}(v_j^{RK},s_{j-1}^*,s_{j+1}^*) > 0.$$

The implicit function theorem applied to $F_{v_j}(v_j^{RK},s_{j-1}^*,s_{j+1}^*)$ asserts the existence of a unique $a_j(s_{j-1})$ and a neighborhood $N_1$ around $s_{j-1}^*$ such that for all $s_{j-1}\in N_1$ we have $F_{v_j}(a_j(s_{j-1}), s_{j-1}, s_{j+1}^*) = 0$, and so

$$RK(s_{j-1},s_{j+1}^*;j) = F(a_j(s_{j-1}),s_{j-1},s_{j+1}^*),$$
$$\left.\frac{\partial RK}{\partial s_{j-1}}\right|_{(s_{j-1},s_{j+1})} =: RK_{s_{j-1}}(s_{j-1},s_{j+1}^*;j) = F_{v_j}(a_j(s_{j-1}),s_{j-1},s_{j+1}^*)a_j'(s_{j-1}) + F_{s_{j-1}}(a_j(s_{j-1}),s_{j-1},s_{j+1}^*),$$
$$RK_{s_{j-1}}(s_{j-1},s_{j+1}^*;j) = \frac{-g_{j,j-1}(a_j(s_{j-1})-E_{syn-e})}{g_{NaP}m_{p,\infty}(a_j(s_{j-1}))(a_j(s_{j-1})-E_{Na})}.$$

Since $a_j(s_{j-1}) - E_{syn-e} < 0$, $a_j(s_{j-1}) - E_{Na} < 0$, and all other terms are positive, we conclude that

$$RK_{s_{j-1}}(s_{j-1},s_{j+1}^*;j) < 0.$$

A similar argument grants that there is a unique function $b_j(s_{j+1})$ and a neighborhood $N_2$ of $s_{j+1}^*$ such that for all $s_{j+1}\in N_2$ we may conclude

$$RK_{s_{j+1}}(s_{j-1},s_{j+1};j) < 0.$$

Similar arguments also yield that the left knee is a monotonically decreasing function of both synaptic inputs. Also, solving $\dot{h_j} = 0$ for $h_j$ yields $h_j = H(v_j)$, the $h_j$-nullcline. The intersection of the $v$- and $h$-nullclines satisfies $F(v_j,s_{j-1},s_{j+1}) - H(v_j) = 0$. For $v_j$ corresponding to the left and right branches of the $v_j$-nullcline, by assumption $F_{v_j}(s_{j-1},s_{j+1}) > 0$, and also by assumption $H_{v_j}(v_j) < 0$, so that the implicit function theorem again applies, yielding a function $\psi(s_{j-1})$ or $\phi(s_{j+1})$, each describing the change of the $v$ coordinate of the fixed point under variation of $s_{j-1}$ or $s_{j+1}$, respectively. Straightforward differentiation yields that $\psi'(s_{j-1}) > 0$ and $\phi'(s_{j+1}) > 0$, and combined again with the fact that the $h_j$-nullcline is a monotonically decreasing function of $v_j$, we see that $\frac{\partial FP}{\partial s_{j-1}}|_{(v_j,s_{j-1},s_{j+1})} < 0$. Similarly, the $h$ coordinate of the fixed point is a monotonically decreasing function of $s_{j+1}$. ■

This result justifies the functional notation in the definitions of $D_Q, D_A, D_T, I_Q, I_A, I_T$ and other terms in Table 1.

The proof we provide for the existence of a periodic orbit corresponding to synchronous bursting relies on the Brouwer fixed point theorem, for which there is a constructive proof.

Theorem 3.2. *Let $D_1, D_2, D_3$ be closed and bounded intervals in $\mathbb{R}^3$. Consider a set $D = D_1\times D_2\times D_3$ and a continuous function $B : D \to D$. There is an $x^*\in D$ such that $B(x^*) = x^*$.*

*Proof.* For the proof of this result, see [16].

**Table 1**

| Symbol | Mathematical definition |
|---|---|
| $D_Q$ | $[RK(s_{max}, s_{max}; Q), RK(0, 0; Q)]$ |
| $D_A$ | $[RK(s_{max}, s_{max}; A), RK(0, 0; A)]$ |
| $D_T$ | $[RK(s_{max}, s_{max}; T), RK(0, 0; T)]$ |
| $\Omega$ | $D_Q \times D_A \times D_T$ |
| $U_Q$ | $[LK(s_{max}, s_{max}; Q), FP(0, 0; Q))]$ valid by (A3) |
| $I_Q$ | $[RK(s_{max}, s_{max}; Q), FP(0, 0; Q))$ |
| $I_A$ | $(FP(s_{max}, s_{max}; A), LK(0, 0; A)]$ valid by (A1) |
| $I_T$ | $(FP(s_{max}, s_{max}; T), LK(0, 0; T)]$ |
| $W$ | $I_Q \times I_A \times I_T$ |
| $\tau_0(h_Q, h_A, h_T)$ | time of flight from $(h_Q, h_A, h_T) \in \Omega$ to $h_T = LK(0, 0; T)$ under the flow $\dot{\overrightarrow{h}} = G_{LLL}(\overrightarrow{h})$ |
| $\tau_{1/3}(h_Q, h_A, h_T)$ | time of flight from $(h_Q, h_A, h_T) \in W$ to $h_A = LK(0, s_T; A)$ under the flow $G_{LLR}(\overrightarrow{h})$; see Figure 16 |
| $\tau^*_{1/3}$ | time of flight from $h_Q \in I_Q, h_T \in I_T, h_A = RK(0, 0; A)$ to $h_A = LK(0, 0, A)$ under the flow $\dot{\overrightarrow{h}} = G_{LLL}(\overrightarrow{h})$, with the additional condition that we hold $s_Q = s_T = 0$ constant; see Figure 17 |
| $\tau_{2/3}(h_Q, h_A, h_T)$ | time of flight from $h_Q \in I_Q, h_T \in (FP(0, 0; T), LK(0, 0; T)], h_A = LK(0, s_T; A)$ to $h_Q = LK(s_T, s_A; Q)$ under the flow $\dot{\overrightarrow{h}} = G_{LRR}(\overrightarrow{h})$; see Figure 18 |
| $\tilde{v}_A$ | $v_A$ corresponding to $h_A = LK(0, 0; A)$ and $s_T = s_{max}$ |
| $\tilde{v}_Q$ | $v_Q$ corresponding to $h_Q = LK(s_{max}, s_{max}; Q)$ and $s_T = s_A = s_{max}$ |
| $\tilde{s}_T$ | $s_T$ corresponding to $h_T = FP(0, 0; T)$, with $v_T = v_{RB}(h_T)$ |
| $\tilde{s}_A$ | $s_A$ corresponding to $h_A = RK(\tilde{s}_T, 0; A)$ for $v_A = v_{RB}(h_A)$ |
| $\tilde{s}_Q$ | $s_Q$ corresponding to $h_Q = RK(\tilde{s}_T, \tilde{s}_A; Q)$ for $v_Q = v_{RB}(h_Q)$ |
| $\tau^*_{2/3}$ | $\tau_h(\tilde{v}_A) \log(LK(0, s_{max}; A)/RK(0, \tilde{s}_T; A))$ |
| $\tau_1(h_Q, h_A, h_T)$ | time of flight from $h_Q \in U_Q$, $h_A \in [LK(0, 0; A), RK(0, s_{max}; A))$, $h_T \in [LK(0, 0; T), FP((s_{max}, 0; T)]$ to $h_Q = RK(s_T, s_A; Q)$ under the flow $\dot{\overrightarrow{h}} = G_{RRR}(\overrightarrow{h})$; see Figure 19 |
| $T_A$ | time of flight from $h_Q \in I_Q$, $h_A = LK(0, 0; A)$, $h_T \in I_T$, to $h_A = RK(0, s_{max}; A)$ under the flow $\dot{\overrightarrow{h}} = G_{RRR}(\overrightarrow{h})$; see Figure 20 |
| $T_T$ | time of flight from $h_Q \in I_Q$, $h_A \in I_A$, $h_T = LK(0, 0; T)$ to $h_T = RK(0, s_{max}; T)$ under the flow $\dot{\overrightarrow{h}} = G_{RRR}(\overrightarrow{h})$ |
| $T_0$ | time of flight from $h_Q \in D_Q, h_A \in D_A$, $h_T = FP(s_{max}, s_{max}; T)$ to $h_T = LK(0, 0; T)$ under the flow $\dot{\overrightarrow{h}} = G_{LLL}(\overrightarrow{h})$ with $s_Q = s_A = 0$ fixed |
| $T_{2/3}$ | $\tau_h(\tilde{v}_Q) \log(RK(s_{max}, s_{max}; Q)/LK(\tilde{s}_A, \tilde{s}_T; Q))$ |
| $T_1$ | time of flight from $h_Q = LK(s_{max}, s_{max}; Q)$, $h_A \in I_A$, $h_T \in I_T$ to $h_Q = RK(\tilde{s}_T, \tilde{s}_A; Q)$ under the flow $\dot{\overrightarrow{h}} = G_{RRR}(\overrightarrow{h})$ with $s_T = s_A = s_{max}$ held constant |

We work in the $\varepsilon = 0$ limit, so that for any particular triple $(h_1, h_2, h_3)$ we precisely know the possible states of the entire solution via the algebraic relations previously mentioned. We will begin by considering the set $\Omega$ consisting of all possible $(h_1, h_2, h_3)$ coordinates where all three cells can enter the silent phase simultaneously, with $v_j = v_j^L(h_j, 0, 0)$ and $s_j = 0$ for all $j$, corresponding to all cells being in the silent phase. We will construct a continuous function $M : \Omega \to \Omega$ by considering the evolution of a trajectory with arbitrary initial condition in $\Omega$ until all cells return to the silent phase. Due to the fact that solutions to ODEs depend continuously on their initial conditions, since $M$ simply evolves a trajectory with initial conditions in $\Omega$, $M$ will be a continuous function. In order to construct $M$ in such a way that it will map $\Omega$

**Table 2**

| Symbol | Interpretation |
|---|---|
| $D_Q$ | range of possible $h$ values at which the $Q$ cell can enter the silent phase |
| $D_A$ | range of possible $h$ values at which the $A$ cell can enter the silent phase |
| $D_T$ | range of possible $h$ values at which the $T$ cell can enter the silent phase |
| $\Omega$ | box containing all possible $(h_T, h_A, h_Q)$ coordinates at which the network can enter the silent phase |
| $U_Q$ | range of possible $h$ values at which the $Q$ cell can enter the active phase |
| $I_Q$ | range of $h$ values that $Q$ can achieve |
| $I_A$ | range of $h$ values that $A$ can achieve |
| $I_T$ | range of $h$ values that $T$ can achieve |
| $W$ | all possible $(h_T, h_A, h_Q)$ coordinates |
| $\tau_0(h_Q, h_A, h_T)$ | the time $T$ takes to enter the active phase, that is, the time for $h_T$ to reach the left knee |
| $\tau_{1/3}(h_Q, h_A, h_T)$ | the time $A$ takes to enter the active phase, taking into account that the position of the left knee changes based on $s_T$ |
| $\tau^*_{1/3}$ | the minimum time $A$ can spend in the silent phase, without input from $T$ |
| $\tau_{2/3}(h_Q, h_A, h_T)$ | the time it takes $Q$ to enter the active phase after $A, T$ have entered the active phase |
| $\tilde{v}_A$ | the maximal value attainable by $v_A$ when only $T$ is in the active phase |
| $\tilde{v}_Q$ | the maximal value attainable by $v_Q$ while $Q$ is still in the silent phase |
| $\tilde{s}_T$ | the minimal synaptic output from cell $T$ when it is in the active phase |
| $\tilde{s}_A$ | the minimal synaptic output from cell $A$ when both $A$ and $T$ are in the active phase |
| $\tilde{s}_Q$ | a lower bound on the minimal synaptic output from cell $Q$ when all three cells are in the active phase |
| $\tau^*_{2/3}$ | the minimal time $A$ can spend in the active phase, if $T$ is also in the active phase |
| $\tau_1(h_Q, h_A, h_T)$ | the time it takes $Q$ to reach its right knee from the time it enters the active phase |
| $T_A$ | maximum time it takes $A$ to reach a point where it will enter the silent phase when $Q$ does |
| $T_T$ | maximum time it takes $T$ to reach a point where it will enter the silent phase when $A$ does |
| $T_0$ | upper bound on the time $T$ can spend in the silent phase |
| $T_{2/3}$ | upper bound on the time $Q$ can spend in the silent phase |
| $T_1$ | a lower bound on the time $Q$ can spend in the active phase |

to $\Omega$, we need estimates on the time it will take each cell to change phases, and it is on these estimates that we will build our assumptions. We note that $M$ can be viewed as a Poincaré map on the three-dimensional section $\Omega$ of the nine-dimensional phase space. The proposition below states that under certain assumptions on times of passage associated with trajectories with initial conditions in $\Omega$, there exists a periodic synchronous bursting solution to (10)–(12). Roughly speaking, the assumptions set an order in which the cells enter the active phase; first $T$ will enter the active phase, then $A$ will follow, and at last $Q$ will enter the active phase before $A$ can return to the silent phase ((A2) and (A3)). Finally, we set an assumption (A4) that will guarantee that all cells enter the silent phase simultaneously, which ensures that $M$ will map $\Omega$ to $\Omega$ (otherwise, a cell that entered the silent phase first might have time to evolve such that its $h$ coordinate leaves $\Omega$). To prove this result, we will show that these assumptions imply that, even in the absolute worst case scenario, every cell will jump from the silent to the active phase before any cell falls from the active to the silent phase and all cells will eventually enter the silent phase together, with respect to the fast time scale.

Rather than writing out each mathematical definition relevant to the proof individually, we have collected these definitions in Table 1. The reader may find it useful to consult this table in conjunction with Table 2, which gives heuristic interpretations of the mathematical definitions.

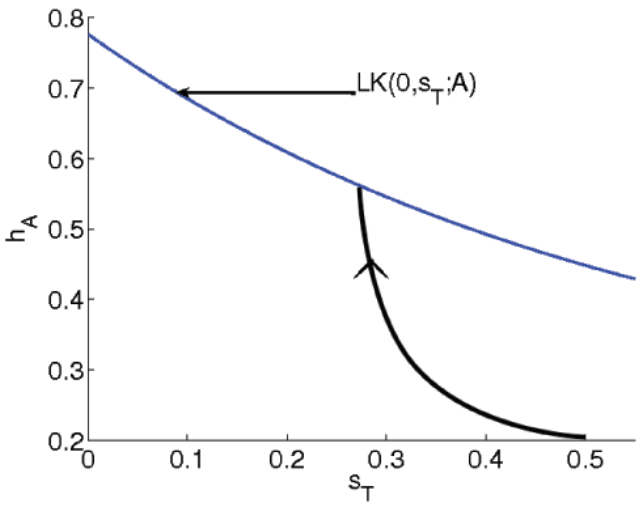


**Figure 16.** *Plot of $h_A$ against $s_T$. The blue curve is the curve of the left knees of the $v_A$-nullcline as a function of $s_T$. When the black trajectory reaches the curve of left knees, the added cell $A$ will jump up to the active phase. The time it takes to reach the curve of left knees is $\tau_{1/3}(h_Q, h_A, h_T)$ for initial conditions $h_Q, h_A, h_T \in W$. In this figure, the blue curve $LK(0, s_T; A)$ was generated numerically for one particular added cell $A$, while the black trajectory is a schematic included for illustrative purposes. For the added cell $A$, all parameters are as in Table 3 in Appendix* A*, except $g_{NaP} = 2, g_L = 2$.*

The reader may also find it illuminating to refer to Figures 16–20 for a graphical representation of some of the critical times involved in the proof of the existence of a synchronous bursting solution given below.

Figure 17 illustrates the definition of $\tau^*_{1/3}$. We have omitted a similar figure for $T_0$. The idea behind these two quantities is that we want to ensure that $T$ enters the active phase before $A$. Therefore, we need to compare the shortest possible time $A$ could take to reach its left knee from the silent phase with the longest possible time $T$ could take to reach its left knee from the silent phase.

Figure 18 illustrates the definition of $\tau_{2/3}(h_Q, h_T, h_A)$. For a given coordinate $(h_Q, h_T, h_A)$ in the silent phase, this gives the time it takes for $Q$ to reach the active phase from that point. An upper bound on $\tau_{2/3}(h_Q, h_T, h_A)$ is given by $T_{2/3}$. This bound must be compared against $\tau^*_{2/3}$, which is the shortest possible time it could take for $A$ to enter the silent phase from the active phase (Figure 19).

Finally, Figure 20 illustrates the quantity $T_A$. As stated above, we will require all cells to enter the silent phase simultaneously, though we prescribe a particular falling order to track the corresponding change in the nullclines. First, $Q$ will enter the silent phase, and then $A$ will follow. For $A$ to be able to enter the silent phase upon the sudden removal of synaptic input from $Q$, the coordinate $h_A$ must be below $RK(0, s_T; A)$, which takes its lowest possible value if $s_T = s_{max}$. Correspondingly, $T_A$ is defined using $RK(0, s_{max})$, as shown in Figure 20. $T_T$ denotes a similar longest active time for the tonic cell, and a similar figure could be generated to illustrate how it is defined. If $T_A$ and $T_T$ are both less than $T_1$, then both the $A$ and $T$ cells will return to the silent phase when $Q$ does.

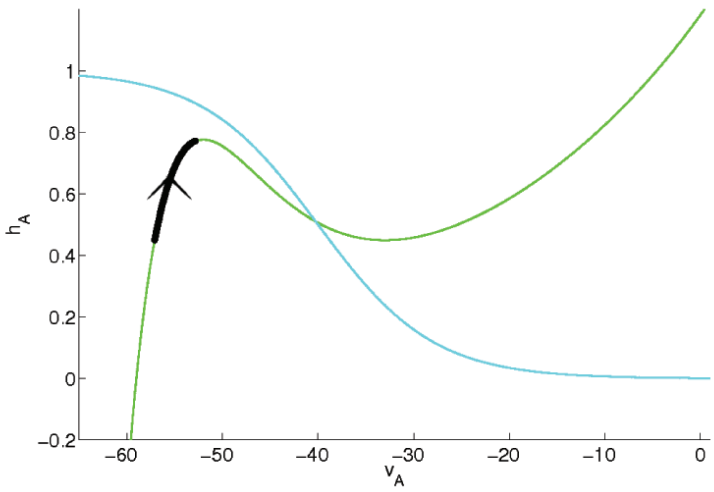


**Figure 17.** *Plot of $h_A$ against $v_A$. The green curve is the $v_A$-nullcline, while the light blue curve is the $h_A$ nullcline. In the worst case, shown here, the trajectory starts as high as possible, namely at $RK(0,0;A)$, and continues to the left knee $LK(0,0;A)$. This evolution takes time $\tau^*_{1/3}$. In this figure, the light blue and green nullclines were generated numerically for a particular choice of the added cell $A$, while the black trajectory is fictive and included for illustrative purposes. For the added cell $A$, the parameters are as in Table 3 in Appendix* A*, except $g_{NaP} = 2, g_L = 2$.*

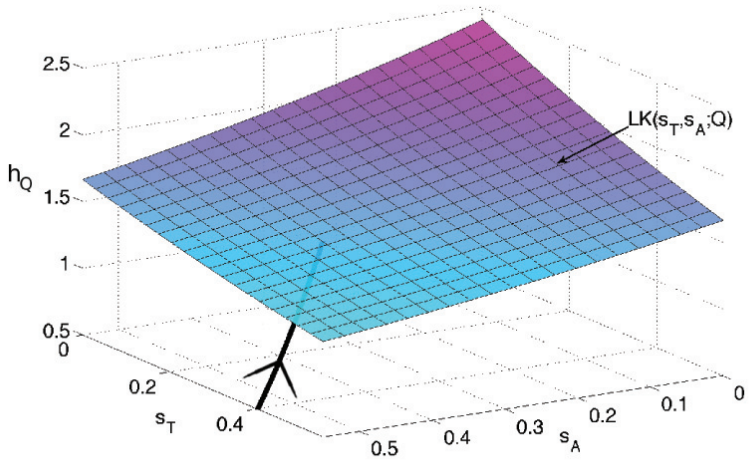


**Figure 18.** *Plot of $h_Q$ against $s_T$ and $s_A$. The multicolored surface is the sheet of $Q$'s left knees as a function of $s_T$ and $s_A$. The black curve is the $h_Q$ coordinate of the $Q$ subsystem under the flow $G_{LRR}(h_Q, h_A, h_T)$. The trajectory evolves towards the sheet as $s_T$ and $s_A$ experience some decay. When trajectory reaches the sheet $LK(s_T, s_A)$, $Q$ enters the active phase. From initial conditions $h_Q, h_A, h_T$, the time it takes the trajectory to reach the sheet is $\tau_{2/3}(h_Q, h_T, h_A)$. In this figure, the sheet of left knees $LK(s_T, s_A; Q)$ for the quiescent cell was generated numerically, while the black trajectory is included for illustrative purposes only. For the quiescent cell $Q$, the parameters are as in Table 3 in Appendix* A*, except $g_{NaP} = 2, g_L = 4$.*

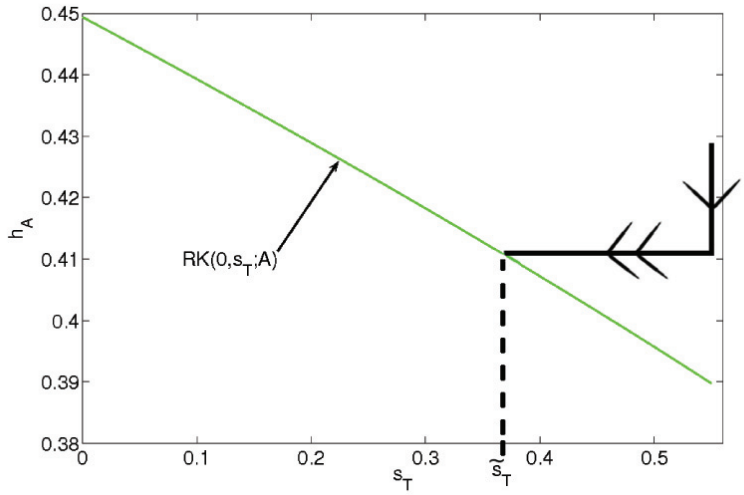


**Figure 19.** *Plot of $h_A$ against $s_T$. The green curve is the curve of right knees of $A$ as a function of $s_T$. The trajectory begins at $LK(0, s_{max})$ and has maximum velocity while $s_T = s_{max}$. The point with the largest value at which $A$ can enter the silent phase is $RK(0, \tilde{s}_T; A)$. $\tau^*_{2/3}$ is defined such that if $s_T$ suddenly dropped to $s_T = \tilde{s}_T$ after time $\tau^*_{2/3}$, then the trajectory of $A$ would exactly hit the curve of knees at $RK(0, \tilde{s}_T; A)$. In this figure, the green curve $RK(0, s_T; A)$ of right knees was generated numerically for a particular choice of the added cell $A$. For the added cell $A$, the parameters are as in Table 3 in Appendix A, except $g_{NaP} = 2, g_L = 2$. The black trajectory is an illustration of the worst-case trajectory and may not be realized.*

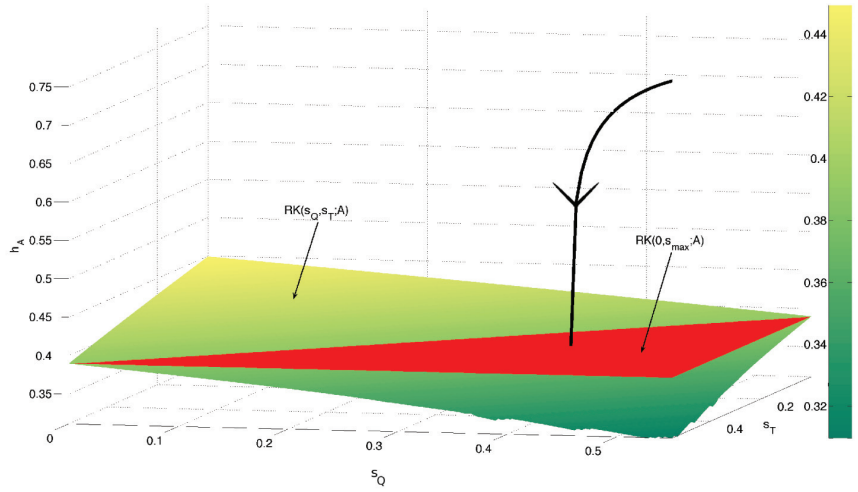


**Figure 20.** *Plot of $h_A$ against $s_T$ and $s_Q$. The green-hued surface is the sheet $RK(s_Q, s_T; A)$ of right knees for $A$ as a function of $s_T$ and $s_Q$. The red plane is $h = RK(0, s_{max}; A)$, the $h$ value of the lowest possible right knee for $A$ when $Q$ has entered the silent phase. In order for $A$ to return to the silent phase simultaneously with $Q$, $h_A$ must be below the red sheet when $Q$ enters the silent phase. We define $T_A$ as the time it takes a trajectory starting from $LK(0, 0; A)$ to reach the red sheet. Here, the green-hued sheet $RK(s_Q, s_T; A)$ and the red sheet $RK(0, s_{max}; A)$ were generated numerically for a particular choice of the added cell $A$. For the added cell $A$, the parameters are as in Table 3 in Appendix A, except $g_{NaP} = 2, g_L = 2$. The black trajectory, on the other hand, is fictive and included for illustrative purposes.*

We make the following assumptions about some of the quantities defined in Table 1:

(A1) Let the added cell $A$ be such that when $s_T = \tilde{s}_T$ and $s_Q = \tilde{s}_Q$ the fixed point for the $A$ subsystem occurs on the right branch of the $v_A$-nullcline.

(A2) $T_0 < \tau^*_{1/3}$.

(A3) $T_{2/3} < \tau^*_{2/3}$.

(A4) $\max(T_A, T_T) < T_1$.

Proposition 3.3. *Under assumptions* (A1)–(A4)*, with the definitions in Table 1, the system of three cells modeled by equations* (10)–(12) *admits a periodic orbit representing synchronous bursting.*

Before stating the proof of the above proposition, we introduce one more bit of notation.

Definition 3.4. *Allow $x \cdot t$ to represent the result of applying the flow of* (10)–(12) *to the initial condition $x$ for $t$ units of model time.*

*Proof.* Assume that (A1)–(A4) hold. Given the definitions in Table 1, the proof is rather concise. First, let $x_0 = (h^0_Q, h^0_A, h^0_T) \in \Omega$. Because $T_0 < \tau^*_{1/3}$ via (A2), $T$ is the first cell to enter the active phase, after time $\tau_0(x_0)$. We then allow $x_1 = x_0 \cdot \tau_0(x_0)$. Since $Q$ is silent under input from $T$, we evolve until $A$ enters the active phase, after an additional time $\tau_{1/3}(x_0)$, and set $x_2 = x_1 \cdot \tau_{1/3}(x_1)$. The condition $T_{2/3} < \tau^*_{2/3}$ of (A3) asserts that $Q$ will always join the active phase before $A$ can fall down to the silent phase. Synaptic input from $A$ lowers $T$'s fixed point. The result of this is that $T$ cannot return to the silent phase until the synaptic input is removed. Thus, we call $x_3 = x_2 \cdot \tau_{2/3}(x_2)$, and after time $\tau_0(x_0) + \tau_{1/3}(x_1) + \tau_{2/3}(x_2)$ all three cells are in the active phase simultaneously. When $Q$ falls down to the silent phase, $h_Q \in D_Q$ by the definition of $D_Q$. Finally, the condition $\max(T_A, T_T) < T_1$ of (A4) asserts that when $Q$ falls down to the silent phase, $h_A \in D_A$ and $h_T \in D_T$, and both $A$ and $T$ will return to the silent phase. If we define $x_4 = x_3 \cdot \tau_1(x_3)$, then we have $x_4 \in \Omega$. Thus, the map $M : x_0 \to x_4$ is a continuous map from $\Omega$ into $\Omega$, and by Brouwer's fixed point theorem there is an $x^*$ such that $M(x^*) = x^*$. Thus, in the $\varepsilon = 0$ limit, the solution with initial condition corresponding to $x^*$ is a periodic orbit. By construction, this orbit meets our definition of a synchronous bursting solution. ∎

Numerical explorations indicate that assumptions (A1)–(A4) are easy to satisfy in the case where two cells are intrinsically tonic and the third is intrinsically quiescent. Parameter sets for which the model satisfied (A1)–(A4), with one cell intrinsically tonic, one intrinsically bursting, and one intrinsically quiescent, were harder to find. An example of such a set consists of the parameter values from Table 3 in Appendix A, except $g_{ij} = 0.0875$, $g_{NaP,1} = 0.795$, $g_{NaP,2} = 1.6945$, $g_{NaP,3} = 0.705$, $g_{L,1} = 0.898$, $g_{L,2} = 1.94709$, $g_{L,3} = 1.209$.

**3.3. Observations on failures to produce synchronous bursts.** In searching for parameter sets for which (A1)–(A4) hold and one cell is intrinsically bursting, the condition $T_{2/3} < \tau^*_{2/3}$ proved to be the hardest to satisfy. While it is true that this condition is fairly restrictive, it reveals a key feature of three-cell networks that include a cell that intrinsically bursts: if the synaptic input from the tonic cell is not strong enough to cause the bursting cell to become tonic itself, then the bursting cell has an opportunity to reenter the silent phase before the quiescent cell can enter the active phase. More precisely, suppose that $s_T = \tilde{s}_T$ and $s_Q = 0$. Suppose that, under the corresponding level of input, the fixed point for cell $A$ falls on the middle branch of the $v_A$-nullcline. In this case, the condition $T_{2/3} < \tau^*_{2/3}$ can

be violated. If this occurs, then there may be an $(h_1, h_2, h_3)$ such that $Q$ fails to enter the active phase before $A$ enters the silent phase, which would violate our necessary conditions for synchronous bursting. In our numerical explorations of these three-cell networks, we identified this premature return to the silent phase as the most common cause for a network to fail to burst synchronously. Addition of a tonic cell instead of a bursting cell ensures that the added cell will not fall down from the active phase to the silent phase before the quiescent cell has a chance to jump up, while addition of a quiescent cell yields a relatively late entry of the added cell into the active phase, which makes it less likely that the original quiescent cell will get stuck in the silent phase.

## 4. Numerical experiments.

**4.1. Implementation.** The numerical results presented in this section were gathered with the MATLAB programming language (The MathWorks, Natick, MA). Equations (10)–(12) are very stiff, and speed became an issue due to the large number of simulations we ran. To speed up our simulations, we used a C implementation of the CVODE package from SUNDIALS [11] for the differential equation integration, compiled as a MATLAB function by way of the mex command.

We allowed a transient of 1000 milliseconds of model time before any conditions on bursting were checked. Typically, integration was done for 10000 milliseconds. When a cell's synaptic output increased beyond 60% of the maximum possible output value, we recorded that the cell entered the active phase. On the other hand, when the cell's synaptic output decreased below 20%, we recorded that the cell entered the silent phase. For purposes of approximating the frequency of synchronous activity, we track each time when all three cells have reentered the silent phase after all three cells have been in the active phase.

The necessary conditions given in section 3.1 provide a guideline for checking whether a solution is synchronous. We implemented these conditions by using a series of Boolean flags that track the states for cells $j+1$, $j-1$ relative to cell $j$. Should a solution fail to meet the necessary conditions at any time after the initial transient, the integration stops and the solution is declared to be asynchronous. One shortcoming of this implementation is that a solution may be declared synchronous if the first time the necessary conditions are violated occurs after 10000 milliseconds. A second shortcoming is that we may be misled by parameter values supporting bistability. Although we cannot guarantee that bistability does not arise, additional numerical explorations suggest that it was rare in the parameter regimes considered.

**4.2. Which cells promote synchronous bursting?** Intuitively, a cell that is intrinsically bursting seems like a safe cell to add to a network to promote synchronous bursting; however, section 3.3 casts doubt on this intuition. We tested this idea more systematically by performing the following numerical experiment. First, pick at random one cell that is intrinsically tonic and another that is intrinsically quiescent. Next, partition $g_{NaP}g_L$ space into a mesh, and use each mesh point to form a third cell to be coupled with the other two into a three-cell network. For each network, integrate (10)–(12) and check whether the network sustains synchronous bursting. We present a colorization of $g_{NaP}g_L$ space as follows. If the third cell failed to create a synchronous burst, we color the coordinate red. Otherwise we color the coordinate

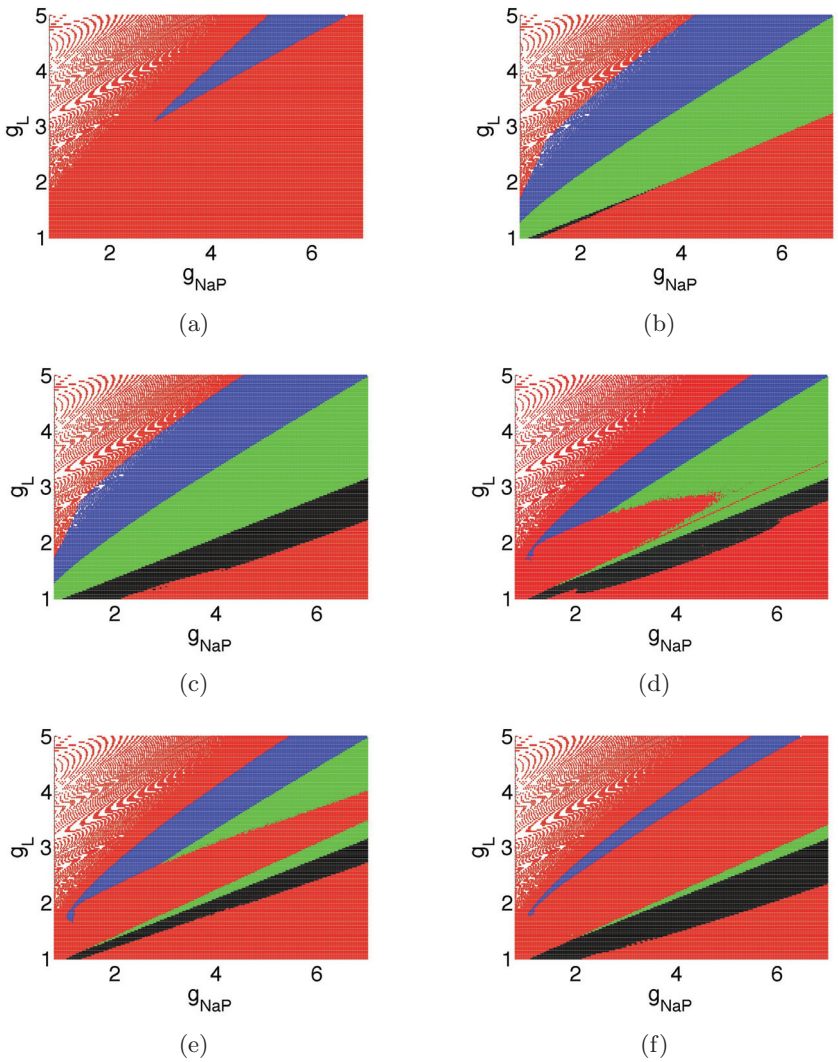


**Figure 21.** *Each panel is a plot of $g_{NaP}$ vs. $g_L$ and represents a numerical experiment with a different pair of fixed intrinsically quiescent and intrinsically tonic cells. For each such experiment, we choose a third cell with parameters $g_{NaP}$ and $g_L$, and color the point $(g_{NaP}, g_L)$ red if the network failed to exhibit synchronous bursting. Otherwise, we color the point according to the added cell's intrinsic dynamics, using blue for quiescent, green for bursting, and black for tonic. For each cell, all parameters are as in Table 3 in Appendix* A*, except that $(g_{NaP,1},\ g_{L,1},\ g_{NaP,2},\ g_{L,2})$ =* (a) (5.772, 1.842, 2.043, 2.552), (b) (4.529, 1.842, 2.043, 2.552), (c) (4.529, 2.236, 5.772, 4.342), (d) (4.529, 2.000, 3.286, 4.105), (e) (4.529, 1.921, 3.286, 4.105), *and* (f) (4.529, 2.000, 5.772, 5.815).

blue if the added cell was intrinsically quiescent, green if it was intrinsically bursting, and black if it was intrinsically tonic. We repeated this experiment with many different random choices of the $Q, T$ pair. After this numerical exploration, certain patterns emerged in these colorizations. In Figure 21, we provide examples that qualitatively cover the breadth of our numerical findings. It may be useful to refer to Figure 2 to recall the division of $g_{NaP}g_L$

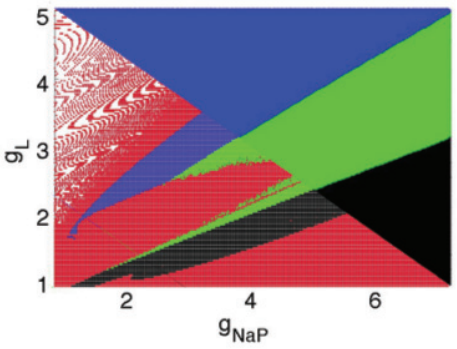


**Figure 22.** *An animated comparison* (76580_01.gif [1.25MB]) *between the original partition of* $g_{NaP}g_L$ *space and one example of the numerical experiment detailed in section* 4.2.

space into regions where the resultant cell is quiescent, bursting, or tonic. We also direct the web-enabled reader to Figure 22 for an animated comparison (76580_01.gif [1.25MB]) between the original partition of $g_{NaP}g_L$ space and one example of the numerical experiment detailed here. A brief analysis of which underlying cell pairs yielded each type of synchronization configuration shown in Figure 21 can be found in Appendix C.

**4.3. Explanation of the mechanisms involved in synchronous bursting.** In each panel of Figure 21, large $g_L/g_{NaP}$ or small $g_L/g_{NaP}$ in the added cell leads to an absence of synchronous bursting in the network. These failures correspond to cases when the third cell is "too quiescent"—that is, even under full input from the other two cells it cannot activate—or "too tonic," in that when input is removed, it cannot transition to the silent phase. Outside of these extreme ranges of $g_L$ and $g_{NaP}$, it was often those coordinates that represent the addition of an intrinsically bursting cell that failed to produce synchronous network-wide bursting. In this section we attempt to explain the mechanisms underlying the changes in network dynamics that occur at the boundaries between the red region and nonred regions of the parameter space.

To explain the results of our experiments, we will for convenience provide arguments based on the positions of the knees of various nullclines. It should be noted that more precise arguments should be expressed in terms of times of flight, as in the proof of the existence of synchronous solutions in section 3.2. However, numerically we observe that the time of flight to the knee in the silent phase is an increasing function of the $h$-coordinate of the left knee and a decreasing function of the $h$-coordinate of the right knee. This result allows an easy translation from knee-based arguments to their time-based analogue.

We consider four basic movements in $g_{NaP}g_L$ space corresponding to increasing or decreasing $g_{NaP}$ or $g_L$ independently. Keeping in mind the insight from section 3.3, that the most common source of network failure is for a cell to prematurely return to the silent phase, we will explain how modulation of $g_{NaP}$ or $g_L$ may affect the bursting behavior of the system. Specifically we are interested in what happens to induce a switch from a red region to a nonred region. That is, we seek to explain the bifurcation from nonsynchronous solutions to synchronous solutions resulting from changes in $g_{NaP}$ or $g_L$.

As we did in section 3.2, we can use the implicit function theorem to write the $h$-coordinates of the left knee and right knee each as a function of $g_L$. By straightforward differentiation of (15), it is then easy to see that the $h$-coordinates of the left and right knees are monotone functions of $g_L$, but an important difference is that the $h$-coordinate of the left knee is much more sensitive to changes in $g_L$, so that for fixed $(h_Q, h_A, h_T) \in W$, $\tau_{1/3}(h_Q, h_A, h_T)$ is a monotonically increasing function of $g_L$. Consider then the crossing from a red region to a nonred region as $g_L$ increases. The result of the added cell having a higher $g_L$ is that it spends more time in the silent phase. This means that the difference between the times when the $A$ and $Q$ cells will enter the active phase is smaller, and thus it is less likely to be the case that $A$ will prematurely return to the silent phase. This explains the transition through the red-nonred border as $g_L$ increases for all the panels in Figure 21, except for Figure 21(b). In Figure 21(b), the only cell within a reasonable parameter regime that could not be successfully added to the network to achieve synchronous bursting was another tonic cell. The explanation for the transition in this case is that the $Q$ for this particular experiment, under synaptic input from the other cells, has a nullcline where the left and right knees have very similar $h$ coordinates. The result is that assumption (A4) is violated. In particular, $T$ will not return to the silent phase with $Q$ each time, because $Q$ does not spend enough time in the active phase for $h_T$ to fall below the $h$-coordinate of the required knee. Increasing $g_L$ to the added cell in this case still causes the $A$ to spend more time in the silent phase, but the beneficial effect is that when $Q$ enters the active phase, $h_T$ is lower and thus more likely to sink below the knee, as required for $T$ to join the silent phase when $Q$ does.

This is not the whole picture, however. Consider those added cells such that when they receive input from a tonic source, they have a fixed point on the right branch of the $v$-nullcline. Such cells will not return to the silent phase until $Q$ first enters the active phase and then returns to the silent phase. If we increase the added cell's value of $g_L$ from such a configuration, it can happen that the intersection of the $v_A$- and $h_A$-nullclines will occur on the middle branch of the $v_A$-nullcline. Suddenly, it becomes possible for $A$ to reenter the silent phase before $Q$ can join the active phase. Reversing this process reveals a mechanism by which lowering $g_L$ for the added cell can allow the network to burst synchronously, and so explains the transition from a red region to a nonred region by lowering $g_L$.

To understand the result of modulation of $g_{NaP}$, we again use the implicit function theorem, but this time we write the $v$-coordinates of the left knee and right knee each as a function of $g_{NaP}$, say $v = \psi(g_{NaP})$. Unfortunately, it is not true that the $h$-coordinates of the knees of a cell are monotonically dependent on $g_{NaP}$, and so our analysis of crossing the red-nonred border is more restricted. Increasing $g_{NaP}$ has the general effect of sliding the $v_A$-nullcline to the left, which causes the intersection with the $h_A$-nullcline to move to the right, possibly causing the intersection point to change from the center to the right branch. We claim that the mechanism for creating synchronous bursting by increasing $g_{NaP}$ is analogous to that generated by lowering $g_L$, consistent with the positive slopes of the boundary curves in Figure 21. That is, increasing $g_{NaP}$ puts the intersection point of the $v_A$- and $h_A$-nullclines for the added cell on the right branch of the $v_A$-nullcline when $T$ is in the active phase. Conversely, lowering $g_{NaP}$ should have an effect analogous to raising $g_L$. Indeed, in the absence of synaptic coupling, lowering $g_{NaP}$ increases the $h$-coordinate of the knees. When $A$ is receiving synaptic input from $T$, the situation is not as obvious. We seek conditions for which the left knee will

increase as $g_{NaP}$ decreases. Allowing $v = \psi(g_{NaP})$ and differentiating (15) with respect to $g_{NaP}$ yields the relation

$$g_L > \frac{-g_{s_{j+1}} s_{j+1}(\psi(g_{NaP}) - E_{syn-e})}{\psi(g_{NaP}) - E_L}. \tag{16}$$

For $g_L$ satisfying (16), the left knee is a monotone decreasing function of $g_{NaP}$ when $T$ is in the active phase. In this case when $g_{NaP}$ is lowered, the left knee's $h$-coordinate again increases more than the right knee's $h$-coordinate, and the analysis is the same as that of the modulation of $g_L$ that we presented previously.

In summary, we identified two primary transitions from asynchronous network dynamics to synchronous network oscillations. One transition mechanism is to eliminate the possibility of the added cell's prematurely entering the silent phase. If the added cell can prematurely return to the silent phase, it must be because, under input from the tonic cell, the intersection of the $v_A$- and $h_A$-nullclines is on the middle branch of the $v_A$-nullcline. When this intersection is moved (by modulation of $g_L$ or $g_{NaP}$) to the right branch of the $v_A$-nullcline, the added cell no longer can return to the silent phase until after the quiescent cell first enters the active phase and then reenters the silent phase. The other transition mechanism involves keeping the quiescent cell in the silent phase for an extended period of time, which allows the tonic cell to approach the intersection of the $v_T$- and $h_T$-nullclines. The closer the tonic cell is to this intersection point, the more likely it is to have its $h$-coordinate sink below the right knee when the quiescent cell returns to the silent phase. The mechanism provided for buying this extra time is not only to make the added cell quiescent, but to ensure that the $h$-coordinate of its left knee is high even under synaptic input from the tonic cell, though not so high that it intersects the $h$-nullcline on the left branch of the $v_A$-nullcline, preventing it from being active. In this way, the quiescent cell and the added cell will spend more time in the silent phase and will enter the active phase at similar times, which prevents one cell from returning to the silent phase before the other cell is ready to follow.

This analysis of the bifurcation from asynchronous network dynamics to synchronous network oscillations reveals what may be called a weakness of a neuron with intrinsically bursting dynamics. When such a bursting cell is added and receives synaptic input from the tonic cell, the intersection of the $v_A$- and $h_A$-nullclines may still be on the center branch of the $v_A$-nullcline. This presents the opportunity for $A$ to enter the silent phase before $Q$ enters the active phase. There are two primary ways to correct this phenomenon. We can increase the $h$-coordinate of $A$'s left knee, thereby giving $Q$ more time to enter the active phase, or we can change the position of $A$'s right knee enough that the intersection of the $v_A$- and $h_A$-nullclines falls on the right branch of the $v_A$-nullcline. Such adjustments are required less frequently for added cells with intrinsically quiescent or tonic dynamics. When a cell is added with intrinsically tonic dynamics, it cannot prematurely return to the silent phase. Therefore the only concern is that $Q$ spends enough time in the active phase to allow $T$ and $A$ to return to the silent phase. On the other hand, if the added cell is intrinsically quiescent, we potentially must still face the issue of $A$ returning to the silent phase before $Q$ enters the active phase. However, the left knees of $Q$ and $A$ have more similar $h$-coordinates than if $A$ were not intrinsically quiescent, and hence the times at which they enter the active phase will differ by less than if $A$ had any other intrinsic dynamics. Therefore it is more likely that $Q$ will

follow $A$ into the active phase. Keeping such results in mind, it is perhaps unsurprising that when adding a third cell to a network already containing a quiescent and tonic cell, it is those added cells which are intrinsically bursting that are most likely to fail to create synchronous oscillations.

**4.4. Which cells promote frequency modulation?** Another important aspect of the preBötC is that it exhibits a wide range of bursting frequencies, perhaps influenced by an outside population of tonically active cells. Biologically, control over frequency for the preBötC would allow it to adapt to changes in environmental and metabolic demands. Further, the system should not be too sensitive to modulation of a control parameter, such as the conductance $g_{ton}$ of the tonic drive current $I_{tonic}$ (i.e., $|\frac{dfrequency}{dg_{ton}}|$ should not be too big). Intuitively, it may seem that a cell that is intrinsically bursting may enhance this dynamic range of network bursting, given that it is naturally tuned to burst. We performed a numerical experiment, however, which suggests that this may not be the case. In our experiment, we repeatedly selected two cells, one intrinsically quiescent and one intrinsically tonic, at random. For each such pair, we added a third cell with $g_{NaP} = 2$ and varied $g_L$ systematically in the interval $(.5, 4)$. Finally, for each value of $g_L$, we varied $g_{ton} \in (0, .25)$, taking $g_{ton} = 0$ as the baseline value without loss of generality. For each $(g_L, g_{ton})$ pair, we recorded the frequency of the network, if it bursted, as the inverse of the average period of synchronous oscillations, recording 0 if synchronous oscillations were not obtained. Figure 23 illustrates some of the results from this experiment.

Our simulations showed that adding an intrinsically bursting cell to the network did not promote synchronous oscillations particularly well, even under modulation of the control parameter $g_{ton}$. Even in those cases where the network demonstrated synchronous oscillations over a wide range of $g_{ton}$ when an intrinsically bursting cell was added, we did not observe a wide range of frequencies for these synchronous oscillations. On the other hand, we saw that adding a quiescent cell often promoted synchronous oscillations under a broad range of $g_{ton}$, and further, when the network produced synchronous oscillations over a wide frequency range, it was commonly an intrinsically quiescent cell that had been added.

**4.5. Explanation of the mechanisms involved in frequency control.** The numerical experiments illustrated in Figure 23 have a trait reminiscent of those in Figure 21: it is common for the network to fail to exhibit synchronous oscillations when the added cell is intrinsically bursting. This experiment gives us information about more than just the existence of synchronous oscillations, however. It also indicates the range of frequencies that the three-cell networks can produce, as well as their robustness to variation of the control parameter $g_{ton}$. We rescaled the parameters relating to the time constants from Butera's original model in [3] to speed up the simulations, so the frequencies recorded here do not match the frequencies seen in the preBötC. However, our qualitative results should carry over to biologically relevant time scales. Based on the criteria discussed in section 4.4, an optimal network should generate a significant color variation extending over a wide range of $g_{ton}$ values. We consistently find that it is the addition of a quiescent cell to the network that allows the network to burst at a wide range of frequencies over a wide range of values of $g_{ton}$.

We offer an explanation for this result by analyzing the $v$-nullclines of the cells. Suppose that we have a network consisting of two quiescent cells and one tonic cell. The control

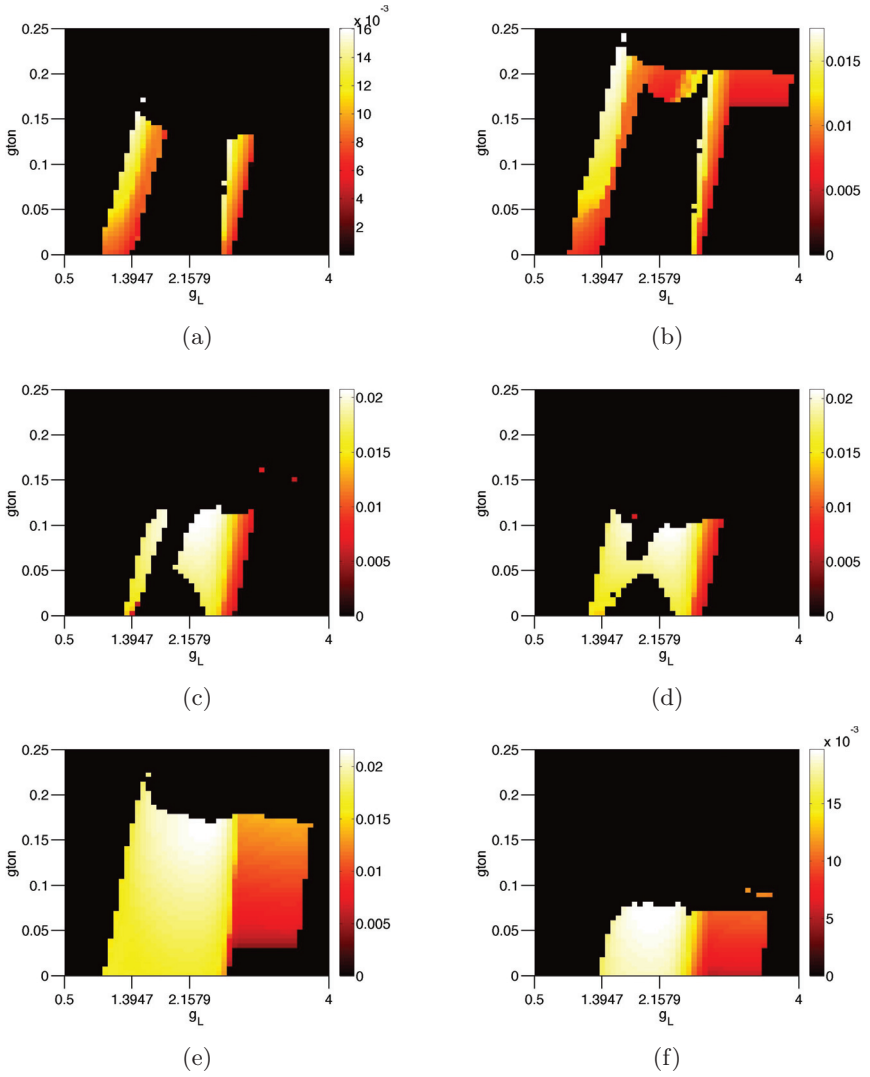


**Figure 23.** *Frequency modulation by $g_{ton}$ depends on the added cell. Each panel shows an individual experiment where an intrinsically quiescent cell and an intrinsically tonic cell were chosen at random. Then, with $g_{NaP} = 2$ and a range of values of $g_L$ between .5 and 4, we added a third cell to the network. For this network, we varied $g_{ton}$ from 0 to .25, and at each mesh point we recorded the average period of synchronous oscillations (recording 0 if synchronous oscillations did not occur). The frequency is color-coded here as the inverse of this average period, unless the period was 0, in which case we recorded the frequency as 0 as well. As indicated on the $g_L$ axis, $g_L = 1.3947$ and $g_L = 2.1579$ represent, for $g_{NaP} = 2$, where the added cell's intrinsic dynamics transition from tonic to bursting and from bursting to quiescent, respectively. The black regions indicate a failure by the network to burst synchronously. The parameters for each cell are as in Table 3 in Appendix A, except $(g_{NaP,1}, g_{L,1}, g_{NaP,2}, g_{L,2})$ = (a) (4.5293, 2.0789, 5.7724, 5.8158), (b) (5.7724, 2.6316, 5.7724, 5.8158), (c) (5.7724, 2.3158, 3.2862, 4.1053), (d) (4.5293, 2.0000, 3.2862, 4.1053), (e) (4.5293, 2.2368, 4.5293, 4.4474), and (f) (5.7724, 2.1579, 4.5293, 4.4474).*

parameter $g_{ton}$ modulates the strength of the excitatory synaptic current $I_{tonic-e}$ in (14), and mathematically, varying $g_{ton}$ is analogous to varying a synaptic conductance variable $s$. Therefore, an argument similar to those in section 3.2 implies that the $h$-coordinate of the left knee of the $v$-nullcline is a monotonic decreasing function of $g_{ton}$. Suppose that input from the tonic cell is insufficient to activate either quiescent cell; that is, they still have their fixed points on the left branches of their $v$-nullclines. Then it is modulation of $g_{ton}$ that can push the knees low enough that one of the quiescent cells can activate through a singular Andronov–Hopf bifurcation where there is an $O(\varepsilon)$ pure imaginary eigenvalue corresponding to the change in the intersection point of the $v$- and $h$-nullclines of the activating cell. In the $\epsilon = 0$ case, for values of $g_{ton}$ beyond this bifurcation but still nearby, the quiescent cell can take arbitrarily long to activate, which yields an arbitrarily low network oscillation frequency. Thus, in the $\epsilon > 0$ case, this slow activation may account for the wide range of frequencies observed, even though arbitrarily low frequencies may no longer be achieved.

Interestingly, in some cases, adding a $T$ cell to a given $(Q, T)$ pair gives a broad range of frequencies similar to that achieved by adding a $Q$ cell, as in Figures 23(a) and 23(b). Let $T$ and $Q$ be the intrinsically tonic and intrinsically quiescent cells fixed for this experiment, and let $A$ be the added cell. We observe that the added cells that yield synchronous oscillations in this experiment for low levels of $g_{ton}$ are either intrinsically tonic or have high values of $g_L$, corresponding to a high value of the $h$-coordinate of the left knee. For intermediate values of $g_L$, a high value of $g_{ton}$ is required to induce the network to burst synchronously. These observations together indicate that the left knee of the quiescent cell has a high $h$-coordinate, even under synaptic input from the tonic cell. With this insight in mind, it makes sense that adding a cell that will become tonic under input from $T$ will provide the $Q$ cell with adequate time to become active over a broad range of $g_{ton}$, with a correspondingly wide range of frequencies of synchronous oscillations. The mechanism for achieving this frequency range will be the same as before: two cells, $A$ and $T$, are stuck in the active phase, so increasing $g_{ton}$ lowers $LK(s_T, s_A; Q)$, which hastens the $Q$ cell's jump to the active phase. As $Q$ jumps into the active phase progressively faster with increased values of $g_{ton}$, the network frequency increases, since $Q$ always controls the network's return to the silent phase. On the other hand, an added cell that is intrinsically quiescent, with the $h$-coordinate of its left knee at a high value similar to that of the $Q$ cell's left knee, will jump up close to the time when $Q$ does, and so also generates synchronous network oscillations.

**5. Discussion.** This work was motivated by the current debate about the source of synchronous rhythmic bursting in the heterogeneous network of cells coupled with synaptic excitation within the preBötC, which includes some intrinsically bursting neurons. It is quite possible that the alternation of the preBötC network between active and silent phases, seen in intact respiratory preparations, is largely controlled by release from and onset of inhibition from outside the preBötC, under some conditions [29, 25]. Nonetheless, it seems clear that bursting emerges from within the preBötC under certain experimental conditions linked to hypoxia or gasping [29, 19, 20]. Previously, it has been shown that cells that intrinsically burst are not required for sustained network-wide bursting in the preBötC [4, 27, 21, 28]. Numerical results do suggest, however, that the presence of neurons that burst under some range of tonic input current does enhance the robustness and frequency range of preBötC bursting. We have furthered this result by explaining why, of all such burst-capable cells, those that are

intrinsically quiescent best support synchronous bursting over a broad frequency range when embedded within a network, as long as intrinsically tonic cells are also present.

To arrive at this conclusion, we provided a definition of synchronous bursting and stated sufficient conditions under which a three-cell network will support a solution that satisfies this definition. To expand upon these results, we numerically explored the effects of adding intrinsically quiescent, bursting, or tonic cells to various (quiescent, tonic) pairs to form various three-cell networks with all-to-all coupling architectures. The central result from these experiments and analysis is that typically, if we start with a network containing an intrinsically quiescent and an intrinsically tonic cell, then it is preferable to add an intrinsically quiescent cell instead of an intrinsically bursting cell to endow the network with the capacity to burst synchronously and to achieve a wide frequency range under variation of the strength $g_{ton}$ of an excitatory synaptic drive. In brief, tonic cells play a key role in spreading synaptic excitation throughout the network and meanwhile remain active, ensuring that all other cells can enter the active phase. Intrinsically bursting neurons can also recruit quiescent cells, but they tend to return to the silent phase too soon, before quiescent cells can become active or before the persistent sodium current for the tonic cells can inactivate sufficiently to allow them to become silent along with the bursters. Intrinsically quiescent cells offer three advantages relative to bursters: because they enter the active phase more slowly, they (a) allow for slower overall burst frequencies to be achieved (see also [7]); (b) provide tonic cells with more inactivation time, decreasing their chances of being stuck in the active phase; and (c) provide extra time for other, even less excitable cells to be recruited to the active phase.

In our simulations, consistent with these features, we observe tightly synchronized transitions from the active phase to the silent phase, whereas the transitions from silent to active may be much less unified. Interestingly, single cells in the preBötC appear to be unable to initiate network bursts, which instead arise through a gradual recruitment [22], reflected in a diversity in active phase onset times observed experimentally [4, 5, 13]. On the other hand, too much spread could pose disadvantages for a strong activation of muscles associated with inspiration; thus, some of the oscillations on the low end of the frequency range that we consider may not be biologically relevant. Clearly, less heterogeneous networks would yield tighter synchronization, but heterogeneity is a known feature of the preBötC. Beyond the possibility that our definition of synchrony is overgenerous, another limitation of our study is the omission of spikes. Spiking effects may make important contributions to preBötC network bursting. For example, two intrinsically tonic preBötC model cells coupled with synaptic excitation may engage in synchronous bursting at a very low frequency, due to asynchrony at the level of spikes within bursts [1]. Nonetheless, our main qualitative result should encompass such spike-related phenomena: to maintain synchronous bursting over a broad range of frequencies, it is optimal to introduce intrinsically quiescent cells into the network, such that a full range of dynamic regimes can be sampled by gradually turning up the strength of the drive (e.g., $g_{ton}$) to these cells, as long as there are enough tonically active cells in the network to recruit the quiescent cells to become active in the first place. Once these cells join the active phase, similar spike asynchrony effects should apply to the network dynamics, regardless of what behavior these added cells exhibited in the absence of coupling.

There are many ways to extend this work. In particular, our work focused on strong excitatory synaptic coupling, and the results may change with weak synaptic excitation, synaptic

inhibition [33], or synaptic plasticity [15]. Further, to understand the dynamics of the preBötC, it is important to realize that the persistent sodium current is not the only mechanism that may yield intrinsically bursting dynamics. Rubin et al. [28] developed a computational model for an experimentally grounded group pacemaker, showing that a calcium-activated nonspecific cation (CAN) current present in at least some cells in the preBötC can give rise to synchronous network bursting that depends crucially on synaptic interactions. As such, an important next step will be to analyze the role of such a group pacemaker within a small heterogeneous network that also includes some cells featuring bursting dependent on the persistent sodium current. It may also be important to understand how the CAN and persistent sodium currents work together within the same cell, to help with the interpretation of various pharmacological experiments.

Another important direction for future work is to consider the effect of noise on the overall dynamics. In particular, a study of which network configurations sustain robust synchronous oscillations in the presence of noise is critical to an understanding of the overall picture of the preBötC. Headway into analysis of noise in the slow-fast dynamics of the preBötC has been made by Nesse, Del Negro, and Bressloff [18].

The preBötC is an example of a central pattern generator (CPG): a network that produces repetitive, multiphasic activity patterns that drive rhythmic motor outputs. CPG rhythms are composed of sequences of synchronous bursts emitted by multiple subnetworks of neurons. Our results could theoretically be relevant to any such subnetwork within the many CPGs identified across a variety of species, as long as its components include conditionally burst-capable neurons, irrespective of the mechanisms responsible for their burst capability (see also [12, 7]). Our conclusions may apply to neural systems other than CPGs as well. For example, our results may be relevant to the generation of gamma oscillations in certain cortical regions, in which rhythmically bursting neurons have been shown to participate [10, 6]. In particular, chattering cells in the visual cortex have been shown in experiments done in vivo to lack intrinsic membrane oscillations in the presence of subthreshold stimuli yet to develop bursting oscillations in response to optimal visual stimuli and to interact with a heterogeneous network of other cell types.

Ultimately, our work identified no significant advantage of adding intrinsically bursting neurons to a network of intrinsically quiescent and intrinsically tonic cells. In this model, modulation of $g_{NaP}$ or $g_L$ switches a cell's intrinsic behavior from quiescent to bursting to tonic, or from tonic to bursting to quiescent. The fact that intrinsically bursting neurons are in the center of this slice of parameter space may account for their presence in the preBötC. Indeed, if there were a similar region of the brain exhibiting network-wide synchronous bursting oscillations, and the mathematical model for the individual cells transitioned under parameter variation from intrinsically quiescent directly to tonic and then to bursting, then we would predict that cells with intrinsically bursting dynamics would not be prominent in the network.

**Appendix A. Function definitions and parameter values.** Below we record the definitions of the individual functions that make up (1)–(4), which were introduced in [3, 4]. In these equations, for $x \in \{h, m, m_P, n, s\}$ the function $x_\infty(v)$ takes the form $x_\infty(v) = \{1 + \exp[(v - \theta_x)/\sigma_x]\}^{-1}$, and also for $x \in \{h, n\}$ the function $\tau_x(v)$ has the form $\tau_x(v) = \bar{\tau}_x / \cosh[(v - \theta_x)/(2\sigma_x)]$. The parameter values used in the simulations are listed in Table 3. These parameters appear as they did in [27], except that we set $\theta_h = -40\,\mathrm{mV}$. Heterogeneity

**Table 3**
*Parameter values for (10)–(12).*

| Parameter | Value | Parameter | Value | Parameter | Value |
|---|---|---|---|---|---|
| $\alpha_s$ | 0.2 ms$^{-1}$ | $I_{app}$ | 12 mV | $\bar{\tau}_h$ | 1 ms |
| $C_m$ | 0.1 pF | $\sigma_h$ | 6 mV | $\bar{\tau}_n$ | 10 ms |
| $E_K$ | −85 mV | $\sigma_m$ | −33 mV | $\tau_s$ | 6.25 ms |
| $E_L$ | −65 mV | $\sigma_{m_P}$ | −5 mV | $\theta_h$ | −40 mV |
| $E_{Na}$ | 50 mV | $\sigma_n$ | −4 mV | $\theta_m$ | −34 mV |
| $E_{syn-e}$ | 0 mV | $\sigma_s$ | −1 mV | $\theta_{mp}$ | −38 mV |
| $g_{ij}$ | 0.35 nS | | | $\theta_n$ | −29 ms |
| $g_{ton}$ | 0 nS | $\varepsilon$ | 1/100 | $\theta_s$ | −33 mV |

was introduced by the parameters $g_{NaP}$ and $g_L$, so they do not appear in Table 3.

**Appendix B. Sufficient conditions for synchronous bursting with alternate architectures and $n \geq 3$ cells.** The conditions presented in section 3.2 applied to a network of three relaxation oscillators. These conditions generalize naturally for a network of $n$ cells, even if the architecture is not all-to-all. Recall that the network as a whole can be thought of as being in one of two stages, "cells moving to the active phase" and "cells moving to the silent phase." Consider a starting set $D_1 \times D_2 \times \cdots \times D_n$, where the $D_j$ are analogous to $D_Q, D_A, D_T$ in Table 1. When the network is in the stage where cells are moving to the active phase, the following rules should be used to generate the sufficient conditions. First, an order in which the cells are going to enter the active phase must be decided upon, and conditions must be placed to ensure that this will be the order for any initial condition on the cross product of possible locations where the cells could reenter the silent phase. Once this order is established, then use $C$ to denote the next cell in line to enter the active phase. Consider $T_C$ to be the longest possible time that $C$ could take to enter the active phase. Next, look at all the cells currently in the active phase. Calculate the fastest-case scenario for a cell to return to the silent phase. As in Figure 19, realize that the $h$-coordinate of a cell in the active phase evolves fastest under maximal input from the other cells in the active phase. If it happened that all synaptic inputs decayed to some minimal value by the time the $h$-coordinate reached the right knee height, the cell would transition to the silent phase. Make this calculation for each active cell, and allow $T_A$ to be the smallest of all these times. Then the sufficient condition becomes $T_C < T_A$. Repeat this process for every cell in the silent phase, each time evolving the network until $C$ enters the active phase.

When the network is returning cells to the silent phase, numerical results suggest an approach to deriving a reasonable set of sufficient conditions for synchrony to be maintained. As in the first case, decide on an order in which the cells will return to the silent phase. Then the sufficient conditions become a cascade; as each cell enters the silent phase, the right knees of all other cells are raised. The sufficient condition is then that the next cell that is to return to the silent phase must be below its new right knee. Repeat this condition for each cell until all of the cells have returned to the silent phase.

This return condition in particular can be relaxed a bit. The Brouwer fixed point theorem requires a map to return a closed set to itself. Thus, if the cells do not return to the silent

phase simultaneously, as long as the last cell enters the silent phase before any cell leaves the starting set, we construct a map that evolves the system until the last cell returns to the silent phase. This map will return the starting set to itself, and so the fixed point theorem yields a fixed point, which will be a periodic orbit of the ODE.

For a network with a different architecture, the same steps as above must be applied. However, care must be taken when determining the order for the cells transitioning between phases. A network other than all-to-all coupling is more complicated because when a cell switches between the active and silent phases, it may not update the nullclines of every other cell in the network. As long as this variation is handled properly in calculating the sheet of knees that each cell must reach to switch phases, the proof does not change. In fact, calculating the fastest time in which a cell can return to the silent phase can be kept the same, again because the $h$ dynamics are fastest under full input. This shortcut may be undesirable; with less than full connectivity the bound will be significantly tighter if the network coupling architecture is incorporated properly.

On the other hand, an architecture including self-coupling may promote synchronous oscillations. We identified in section 3.3 that intrinsically bursting cells that do not become tonic under synaptic input from the tonic cell may prematurely fall down to the silent phase before the rest of the network can join the active phase. However, should these intrinsically bursting cells provide synaptic input to themselves, that extra kick may be enough to push their critical point to the right branch, inducing a tonic behavior. As long as the intrinsically quiescent cell can fall down to the silent phase under full synaptic input, the all-to-all architecture with self-coupling should support synchronous oscillations more robustly than the architecture considered throughout this work.

**Appendix C. Additional analysis for section 4.2.** Figure 24 highlights an auxiliary experiment designed to increase our understanding of the relative frequency of occurrence of the various configurations represented by the individual panels of Figure 21, and of which pairs of intrinsically quiescent and intrinsically tonic cells give rise to each configuration. For the numerical experiment, we selected a set of intrinsically quiescent and intrinsically tonic cells. For each pair, we explored network dynamics over a range of added cell parameters, as in section 4.2, and produced a diagram of the results, as for Figure 21. We qualitatively categorized each pair based on the similarity of the resulting diagram to the individual panels from Figure 21. Figure 24 illustrates the pairs identified for two such panels.

One result of this experiment is that, for each panel in Figure 21, $Q$ cells with diverse $(g_{NaP}, g_L)$ values appear to generate similar synchrony configurations, and they do so by pairing with different $T$ cells. This observation suggests that there may be multiple mechanisms through which each configuration represented in Figure 21 can arise. Interestingly, the ratio $\frac{g_L}{g_{NaP}}$ for the quiescent cell seems to be important in selecting the configuration that results, although the parameters for the $T$ cell contribute as well.

We performed one more simulation to investigate this idea further. For each category from the above numerical experiment, we took the average value of $g_L$ for the intrinsically quiescent cells together with the average value of $g_{NaP}$ for those cells, to form an average intrinsically quiescent cell. Similarly, we formed an average intrinsically tonic cell for that category. Then we performed the simulation from section 4.2.

We found that in several cases the results from the intrinsically quiescent and intrinsically

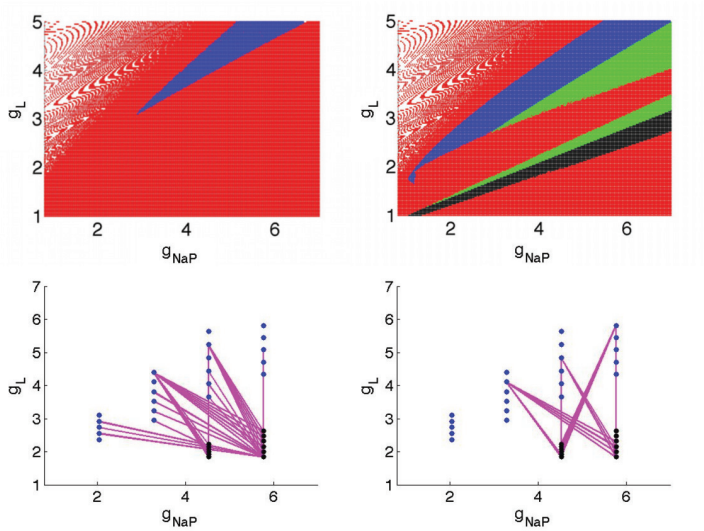


**Figure 24.** *An illustration of which pairs of (Q,T) cells give rise to two classes of synchrony outcomes. The top row shows two examples from Figure 21. In the bottom row, dots corresponding to quiescent cells are blue, and dots corresponding to tonic cells are black. In each panel, the dots for each intrinsically quiescent and intrinsically tonic pair are connected if, using the procedure discussed in section 4.2, this pair generated a synchrony diagram like the one in the panel above.*

tonic pair generated with the averaged parameters did not match those generated from the individual pairs that were averaged. While this result may initially seem surprising, it reflects the fact that there may be multiple clusters of pairings that produce each configuration, whereas the average across all relevant pairs may lie outside all such clusters.

**Acknowledgments.** The authors would like to thank Ernest Barreto and David Terman for their useful suggestions related to Appendix C.

## REFERENCES

[1] J. Best, A. Borisyuk, J. Rubin, D. Terman, and M. Wechselberger, *The dynamic range of bursting in a model respiratory pacemaker network*, SIAM J. Appl. Dyn. Syst., 4 (2005), pp. 1107–1139.

[2] A. Bose, N. Kopell, and D. Terman, *Almost-synchronous solutions for mutually coupled excitatory neurons*, Phys. D, 140 (2000), pp. 69–94.

[3] R. Butera, J. Rinzel, and J. Smith, *Models of respiratory rhythm generation in the pre-Botzinger complex.* I. *Bursting pacemaker neurons*, J. Neurophysiol., 82 (1999), pp. 382–397.

[4] R. Butera, J. Rinzel, and J. Smith, *Models of respiratory rhythm generation in the pre-Botzinger complex.* II. *Populations of coupled pacemaker neurons*, J. Neurophysiol., 82 (1999), pp. 398–415.

[5] R. Butera, J. Rubin, D. Terman, and J. Smith, *Oscillatory bursting mechanisms in respiratory pacemaker neurons and networks*, in Bursting: The Genesis of Rhythm in the Nervous System, S. Coombes and P. Bressloff, eds., World Scientific, Singapore, 2006, pp. 303–346.

[6] M. Cunningham, M. Whittington, A. Bibbig, A. Roopun, F. LeBeau, A. Vogt, H. Monyer, E. Buhl, and R. Traub, *A role for fast rhythmic bursting neurons in cortical gamma oscillations in vitro*, Proc. Natl. Acad. Sci. USA, 101 (2004), pp. 7152–7157.

[7] S. Daun, J. Rubin, and I. Rybak, *Control of oscillation periods and phase durations in half-center central pattern generators: A comparative mechanistic analysis*, J. Comput. Neurosci., 27 (2009), pp. 3–36.

[8] J. Feldman and C. Del Negro, *Looking for inspiration: New perspectives on respiratory rhythm*, Nature Rev. Neurosci., 7 (2006), pp. 232–241.
[9] N. Fenichel, *Geometric singular perturbation theory for ordinary differential equations*, J. Differential Equations, 31 (1979), pp. 53–98.
[10] C. Gray and D. McCormick, *Chattering cells: Superficial pyramidal neurons contributing to the generation of synchronous oscillations in the visual cortex*, Science, 274 (1996), pp. 109–113.
[11] A. Hindmarsh, P. Brown, K. Grant, S. Lee, R. Serban, D. Shumaker, and C. Woodward, *SUNDIALS: Suite of nonlinear and differential/algebraic equation solvers*, ACM Trans. Math. Software, 31 (2005), pp. 363–396.
[12] E. Izhikevich, *Dynamical Systems in Neuroscience: The Geometry of Excitability and Bursting*, MIT Press, Cambridge, MA, 2007.
[13] S. Johnson, J. Smith, G. Funk, and J. Feldman, *Pacemaker behavior of respiratory neurons in medullary slices from neonatal rat*, J. Neurophysiol., 72 (1994), pp. 2598–2608.
[14] C. Jones, *Geometric singular perturbation theory*, in Dynamical Systems (Montecatini Terme, 1994), Lecture Notes in Math. 1609, Springer, Berlin, 1995, pp. 44–118.
[15] J. Karbowski and G. Ermentrout, *Synchrony arising from a balanced synaptic plasticity in a network of heterogeneous neural oscillators*, Phys. Rev. E, 65 (2002), paper 31902.
[16] R. B. Kellogg, T. Y. Li, and J. Yorke, *A constructive proof of the Brouwer fixed-point theorem and computational results*, SIAM J. Numer. Anal., 13 (1976), pp. 473–483.
[17] A. Kolesov, E. Mishchenko, and N. Rozov, *Asymptotic methods of investigation of periodic solutions of nonlinear hyperbolic equations*, Trudy Mat. Inst. VA Steklova, 222 (1998), pp. 7–191.
[18] W. Nesse, C. Del Negro, and P. Bressloff, *Oscillation regularity in noise-driven excitable systems with multi-time-scale adaptation*, Phys. Rev. Lett., 101 (2008), paper 088101.
[19] J. Paton, A. Abdala, H. Koizumi, J. Smith, and W. St-John, *Respiratory rhythm generation during gasping depends on persistent sodium current*, Nature Neurosci., 9 (2006), pp. 311–313.
[20] F. Peña, M. Parkis, A. Tryba, and J. Ramirez, *Differential contribution of pacemaker properties to the generation of respiratory rhythms during normoxia and hypoxia*, Neuron, 43 (2004), pp. 105–117.
[21] L. K. Purvis, J. C. Smith, H. Koizumi, and R. J. Butera, *Intrinsic bursters increase the robustness of rhythm generation in an excitatory network*, J. Neurophysiol., 97 (2007), pp. 1515–1526.
[22] J. Ramirez, A. Tryba, and F. Pena, *Pacemaker neurons and neuronal networks: An integrative view*, Current Opinion Neurobiol., 14 (2004), pp. 665–674.
[23] P. Rowat and A. Selverston, *Synchronous bursting can arise from mutual excitation, even when individual cells are not endogenous bursters*, J. Comput. Neurosci., 4 (1997), pp. 129–139.
[24] J. Rubin and K. Josic, *The firing of an excitable neuron in the presence of stochastic trains of strong synaptic inputs*, Neural Comput., 19 (2007), pp. 1251–1294.
[25] J. Rubin, N. Shevtsova, B. Ermentrout, J. Smith, and I. Rybak, *Multiple rhythmic states in a model of the respiratory CPG*, J. Neurophysiol., 101 (2009), pp. 2146–2165.
[26] J. Rubin and D. Terman, *Geometric singular perturbation analysis of neuronal dynamics*, in Handbook of Dynamical Systems 2, Elsevier Science, 2002, pp. 93–146.
[27] J. E. Rubin, *Bursting induced by excitatory synaptic coupling in nonidentical conditional relaxation oscillators or square-wave bursters*, Phys. Rev. E, 74 (2006), paper 021917.
[28] J. E. Rubin, J. Hayes, J. Mendenhall, and C. Del Negro, *Calcium-activated nonspecific cation current and synaptic depression promote network-dependent burst oscillations*, in Proc. Natl. Acad. Sci. USA, 106 (2009), pp. 2939–2944.
[29] J. Smith, A. Abdala, H. Koizumi, I. Rybak, and J. Paton, *Spatial and functional architecture of the mammalian brainstem respiratory network: A hierarchy of three oscillatory mechanisms*, J. Neurophysiol., 98 (2007), pp. 3370–3387.
[30] J. Smith, H. Ellenberger, K. Ballanyi, D. Richter, and J. Feldman, *Pre-Botzinger complex: A brainstem region that may generate respiratory rhythm in mammals*, Science, 254 (1991), pp. 726–729.
[31] D. Somers and N. Kopell, *Rapid synchronization through fast threshold modulation*, Biolog. Cybernet., 68 (1993), pp. 393–407.
[32] D. Terman, N. Kopell, and A. Bose, *Dynamics of two mutually coupled slow inhibitory neurons*, Phys. D, 117 (1998), pp. 241–275.
[33] J. White, C. Chow, J. Rit, C. Soto-Trevino, and N. Kopell, *Synchronization and oscillatory dynamics in heterogeneous, mutually inhibited neurons*, J. Comput. Neurosci., 5 (1998), pp. 5–16.